

## **Section 1**

Assimilation of atmospheric and land observations.

Data impact and sensitivity studies.

Methodological advances.



# Development of Ground-Based Microwave Radiometer Network and Monitoring System using 1-Dimensional Variational Technique

Kentaro Araki<sup>1</sup>, Hiromu Seko<sup>1</sup>, Hiroshi Ishimoto<sup>1</sup>, Takuya Tajiri<sup>1</sup>, Koichi Yoshimoto<sup>2,1</sup>, Makoto Matsumoto<sup>2</sup>, Tomohiro Takeda<sup>2</sup>, Yoshiyuki Kawano<sup>2</sup>, Kenji Suzuki<sup>2</sup>, Kazumasa Nakayama<sup>2</sup>

1: Meteorological Research Institute, Tsukuba, Ibaraki, Japan

2: Japan Meteorological Agency, Minato-ku, Tokyo, Japan

e-mail: araki@mri-jma.go.jp

## 1. Introduction

In Japan, landslides and flash floods are often caused by quasi-stationary convective bands (QSCBs) during the rainy season, and many previous studies have pointed out the importance of large amounts of water vapor supply in the lower atmosphere in the formation of QSCBs. Therefore, the Japan Meteorological Agency (JMA) has been enhancing water vapor observations in order to improve the monitoring and forecasting techniques for QSCBs and to elucidate the mechanism of QSCBs. As part of this effort, we have established a network of ground-based microwave radiometers (MWRs) in FY2022 and developed a system for real-time monitoring using data assimilation methods. In this report, we describe the outline of the MWR observation network and monitoring system, the verification results of vertical profiles of air temperature and water vapor density, and the initial observation results including precipitation cases.

## 2. Microwave radiometer network

First, RPG-HATPRO-G5 was adopted for this MWR observation network. This MWR observes brightness temperature at intervals of 1 second to several minutes with 7 channels in the 22 to 31 GHz band sensitive to water vapor and cloud water, and 7 channels in the 51 to 58 GHz band sensitive to oxygen. Based on this data, vertical profiles of temperature and water vapor density can be estimated using neural networks (NNs) and data assimilation methods developed at the Meteorological Research Institute (MRI).

We have installed MWRs at 17 stations, mainly in western Japan where heavy rainfall due to QSCBs and typhoons is likely to occur. An overview of the stations and the MWR observation network are shown in Figs. 1 and 2. Observation sites were chosen where the JMA had already installed wind profilers. This allows us to obtain atmospheric thermodynamic profiles of air temperature and water vapor density and dynamic profiles of wind at the same time.



Figure 1. Overview of MWR station at Owase. The equipment in the foreground is MWR and the one in the background is WPR.

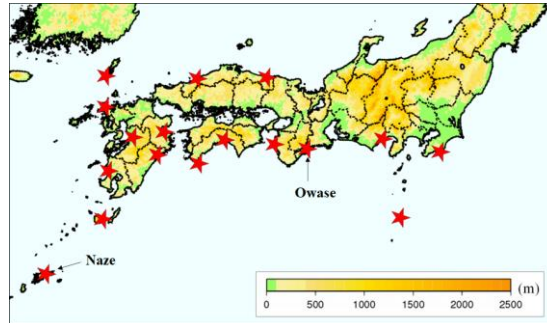


Figure 2. MWR Observation Network. Red stars mean MWR observation points. Paint color indicates elevation (m).

## 3. Monitoring system using 1DVAR technique

The NN has been widely used as a retrieval method for temperature and water vapor density using MWR data. On the other hand, it has been pointed out that NN has large errors, especially in the upper atmosphere. Therefore, our group at the MRI have developed a vertical one-dimensional variational data assimilation method (1DVAR) that combines numerical weather model results with MWR data and verified that its accuracy is better than that of NN and model results (Araki et al., 2015).

In this study, a new 1DVAR method was developed at JMA based on MRI's 1DVAR. In addition to MWR data, this method assimilates JMA surface meteorological observations of temperature and water vapor and wind data from wind profilers. In the 1DVAR of this study, 48 vertical layers were calculated from the ground to an altitude of about 21 km, and the analysis variables were temperature, pseudo-relative humidity, and wind. The LBFSGS method, which is also used for JMA mesoscale analysis, was applied for the minimum value search. The results of the JMA operational mesoscale model (MSM) were used as the first estimate (Guess), and the 1DVAR analysis was performed every 10 minutes in real time at all MWR stations.

To verify the accuracy of the 1DVAR, we compared it with the results of the July-August 2022 sonde observations at Naze (Fig. 3) when no rain was observed within 1 hour before and after sonde observations, since rain causes errors in MWR observations. The results showed that for temperature, the bias (mean difference: MD) and root-mean-square (RMS) difference were smaller for 1DVAR than for NN and Guess. For water vapor density,

the MD and RMSE of 1DVAR were smaller than those of NN and Guess. This confirms that 1DVAR with MWR data can be used to obtain highly accurate temperature and water vapor profiles.

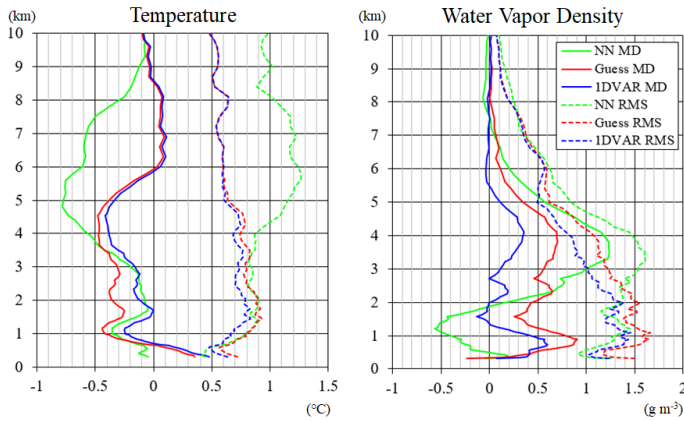


Figure 3. Accuracy of profiles for temperature and water vapor density, based on 1DVAR, first guess of MSM (Guess) and neural network (NN) profiles based on observations at Nase during July and August 2022. The bias (Mean Difference: MD, solid line) and variability (RMS, dashed line) of each profile with respect to the sonde observations are shown for temperature on the left and for water vapor density on the right. 100 cases without rain within 1 hour before or after the time of the sonde observation are used for verification.

#### 4. Case study on monitoring atmospheric conditions

As the initial results of the MWR monitoring system, Fig. 4 shows the temporal changes in precipitable water vapor (PWV) and CAPE at Nase from July 5 to 11, 2022. Note that it is difficult to compare absolute values due to the different elevations of the MWR, sonde (Sonde), and model (Guess). The trends of PWV and CAPE obtained from Sonde, 1DVAR, and NN are in good agreement, and the variations in PWV and CAPE that cannot be expressed by Guess (e.g., 09-15 JST (= UTC+9h) on July 7, yellow arrow in Fig. 4) can be expressed by 1DVAR and NN. This result suggests that the MWR data captures abrupt changes in atmospheric conditions well.

On July 9, 2022, the MWR at Nase observed inflows to the developed precipitation system (orange arrow period in Fig. 4). Temporal variations of atmospheric conditions based on 1DVAR analysis are shown in Fig. 5. Precipitation was observed around 15 JST on 9, and the water vapor flux increased in the lower atmosphere below 1 km altitude until around this time. Correspondingly, the water vapor density in the lower atmosphere also increased, resulting in a rapid instability of the atmospheric conditions. After the precipitation, the water vapor density in the lower atmosphere increased, but the amount of precipitable water rapidly decreased due to the inflow of air with a low equivalent potential temperature (EPT) into the middle atmosphere.

From these results, the monitoring system using MWR data and the 1DVAR technique would be beneficial for real-time monitoring of atmospheric conditions in severe weather.

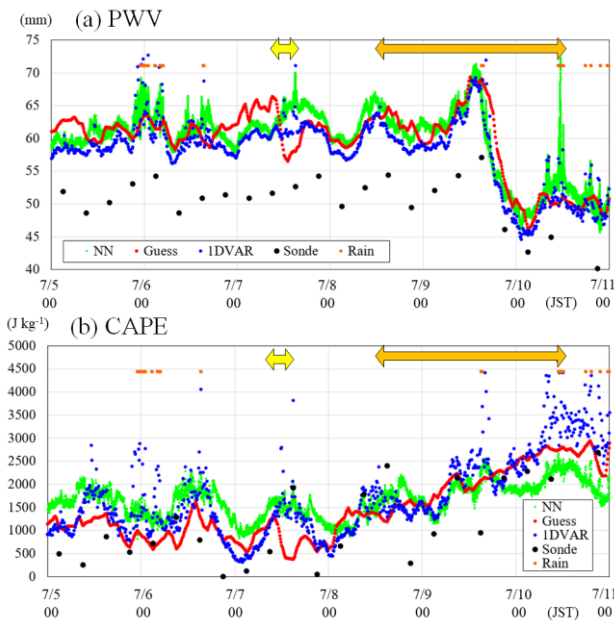


Figure 4. Time series of (a) precipitable water vapor (PWV) and (b) CAPE at Nase for July 5-11, 2022. Dots represent NN in green, Guess in red, 1DVAR in blue, and sonde observations in black. Orange dots mean rain. The elevations of the MWR and Sonde stations, and Guess are 3 m, 295 m, and 53 m, respectively.

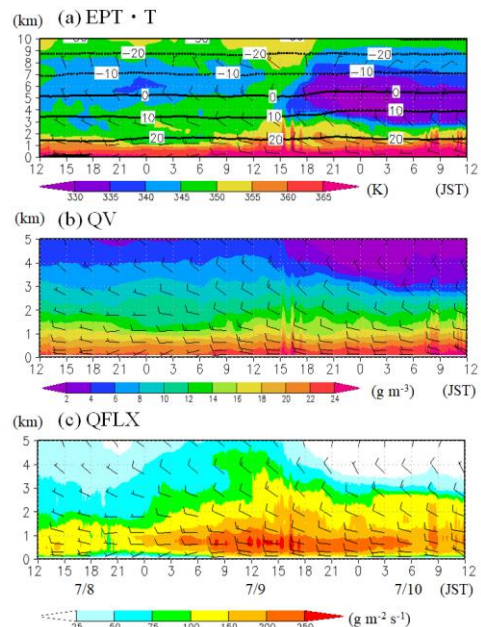


Figure 5. Time-height cross sections of the environmental field at Nase from 12 (JST) on 8 to 12 (JST) on 10 July 2022, obtained from 1DVAR analyses of (a) EPT (K, shaded) and temperature ( $^{\circ}\text{C}$ , contours), (b) water vapor density (QV,  $\text{g m}^{-3}$ ), and (c) water vapor flux (QFLX,  $\text{g m}^{-2} \text{s}^{-1}$ ). Barbs indicate horizontal wind derived from 1DVAR analysis.

#### References:

Araki, K., M. Murakami, H. Ishimoto, and T. Tajiri, 2015: Ground-based microwave radiometer variational analysis during no-rain and rain conditions. *SOLA*, **11**, 108–112.

# Assimilation of Indian DWR Radial Velocity in Regional NCUM-R Model

Devajyoti Dutta\*, Ashish Routray, John P. George and V. S. Prasad

National Centre for Medium Range Weather Forecasting (NCMRWF), Ministry of Earth Sciences (MoES),  
A-50, Sector-62, Noida UP-201309, India

\*E-mail address: [djyoti@ncmrwf.gov.in](mailto:djyoti@ncmrwf.gov.in)

## 1. Introduction:

The need for precise forecasting of severe weather events over the Indian region is on the rise. Over the past years, significant enhancements have been made in improving the predictability of high-impact weather events through the implementation of higher model resolutions (Dutta et al., 2018 & 2019). Prior research conducted by many authors has provided evidence of the beneficial impact of assimilating Doppler Weather Radar (DWR) data in the high-resolution Numerical Weather Prediction (NWP) systems, particularly of convective-permitting scales. These studies have shown positive outcomes in terms of influencing structural fields, which in turn have the potential to enhance the accuracy of convection evolution and precipitation forecasts. Here we are presenting a case study which represents some of the efforts of National Centre for Medium Range Weather Forecasting (NCMRWF, India) for improving the high resolution NWP forecast by including the Indian DWR datasets in its high-resolution regional NWP system.

The NCMRWF Unified Model (NCUM-R) is currently in operational at NCMRWF with a horizontal grid spacing of approximately 4 km, encompassing 1200 x 1200 grid points and 80 vertical level within the domain. In this study, the regional data assimilation system utilizes the 4DVAR (Four-Dimensional Variational) method to generate the initial conditions for the NCUM-R forecast model (Courtier et al. 1994). To assess the beneficial impact of DWR radial velocity assimilation, a case study (26–29 July 2016) is presented. This period represents an active period of south-west monsoon season, with heavy to very heavy rainfall occurred over many parts of India. Two numerical experiments are carried out viz. CNTL (assimilation of convective and non-convective observations) and RAD (assimilation of observations in CNTL plus DWR radial velocity).

## 2. Results:

The Quality Control (QC) procedures are developed for DWR radial velocity which involves analyzing the standard deviation and non-meteorological echoes in the DWR radial velocity data to identify and eliminate low-quality data. To ensure data accuracy, an Observation Processing System (OPS) is employed for further quality control. Following the OPS procedure, Super Observations are generated by combining the nearby observations. Figure 1a–c illustrates the raw observations obtained from the Chennai DWR station, including the deviation of the observation from the background ( $O - B$ ), as well as the super-observations utilized in the assimilation cycle respectively. In the assimilation cycle, DWR observations from 12 stations in India operating in varying frequency bands (S-band, C-band, and X-band) were considered. The details of the DWR stations over Indian region are shown in Figure 1d. Figure 2a–c presents the merged data from Global Precipitation Measurement (GPM) satellite-rain gauges and 24-hour accumulated rainfall from both simulations. The RAD experiment (Figure 2c) effectively simulates the rainfall amount and spatial distribution across all regions compared to the CNTL experiment (Figure 2b). Figure 2d displays the time series of 1-hourly accumulated model-simulated rainfall from the CNTL and RAD analyses, along with observations from the GPM satellite. It is evident from the figure that the RAD simulation closely matches with the rainfall pattern observed by GPM throughout the forecast hours in all cases. In summary, the RAD experiment demonstrates better performance in simulating rainfall patterns and closely aligning with observations, offering valuable insights into analysis forecast system and understanding precipitating system in the studied regions.

## References:

Courtier, P., Thépaut, J. N., & Hollingsworth, A. (1994). A strategy for operational implementation of 4D-Var, using an incremental approach. *Quarterly Journal of the Royal Meteorological Society*, 120(519), 1367–1387.

Dutta, D., Routray, A., Preveen Kumar, D., George, John P., & Singh, V. (2018). Simulation of a heavy rainfall event during southwest monsoon using high-resolution NCUM-modeling system: A case study. *Meteorology and Atmospheric Physics*. 131, pages1035–1054 (2019).

Dutta D, Routray A, Preveen Kumar D, George JP (2019) Regional data assimilation with the NCMRWF unified model (NCUM): impact of doppler weather radar radial wind. *Pure Appl Geophys* 176:4575–4597.

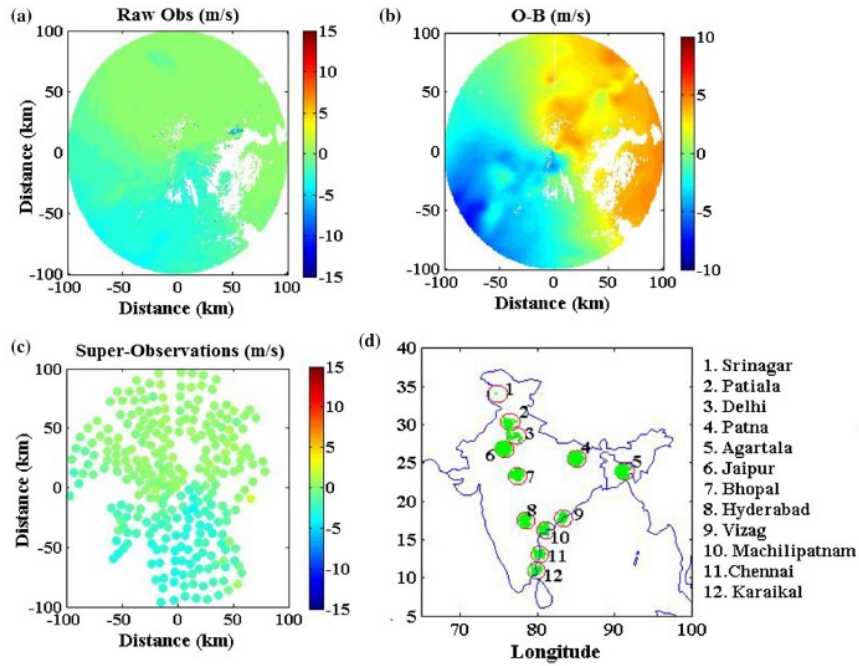


Fig 1: a) Raw DWR observation; b) observed minus background (O – B); c) super-observations from the Chennai DWR station (as an example on 00 UTC 26 July 2016); d) DWR stations (color in the circle represent the amount of observations received).

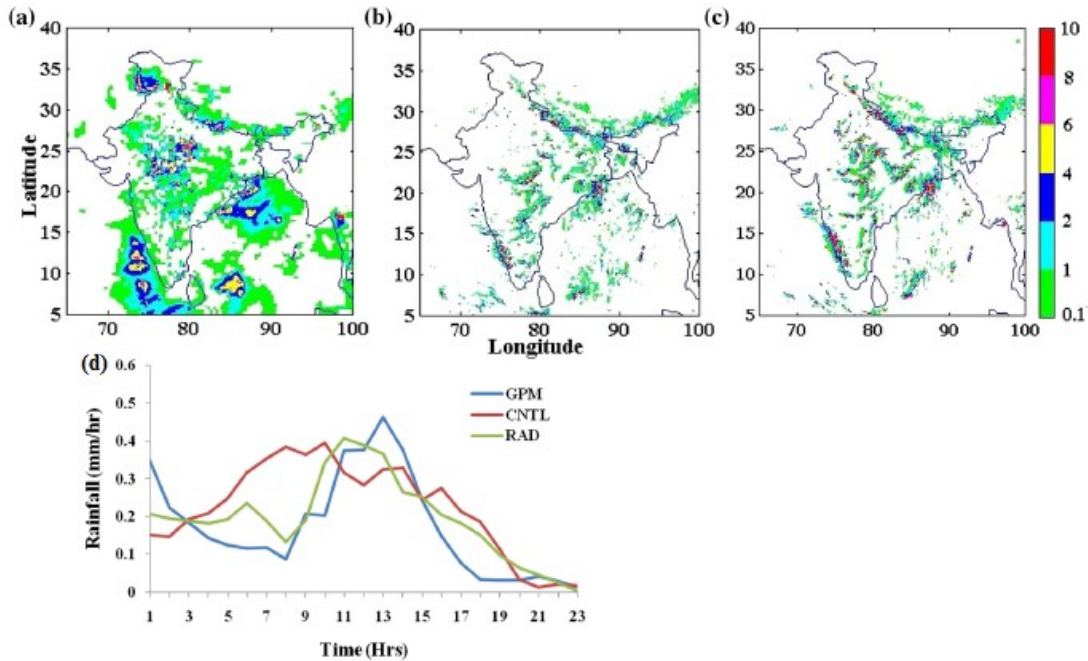


Fig 2: Twenty four hours of accumulated rainfall (cm) of 26<sup>th</sup> July 2016 from a) merged satellite-rain gauge analysis (NCMRWF-IMD), b) CNTL and c) RAD for day 1 valid at 03 UTC 27 July 2016 d) Hourly variation of area-averaged (20<sup>o</sup>–37<sup>o</sup>N; 75<sup>o</sup>–82<sup>o</sup> E) rainfall of day 1 from GPM, CNTL and RAD simulations of 27 July 2016.

# Implementation of WRF based High Resolution Rapid Refresh system over East Indian Region

K.B.R.R. Hari Prasad\*, Ashish Routray, SuryaKanti Dutta, Greeshma M Mohan and V.S. Prasad

National Centre for Medium Range Weather Forecasting (NCMRWF), Ministry of Earth Sciences (MoES), A-50, Sector-62,  
Noida UP-201309, India

\*E-mail address: [kbr.hari@gov.in](mailto:kbr.hari@gov.in), [kbrhari@gmail.com](mailto:kbrhari@gmail.com)

## 1. Introduction

To mitigate the significant threat to human life and property due to the highly localized severe weather systems high-resolution more accurate forecasts are needed. The high-resolution convection allowing NWP models ( $\leq 3$  km) fulfill this demand. The isolated and highly localized convective features are well monitored by convective scale measurements such as Doppler Weather Radars (DWR), lightning detection networks etc. The information related to the presence of deep, moist, and mixed-phase convective activities from these sources can be utilized to improve the model's initial fields and produce better short-term forecasts (Kong et al., 2018). The High-Resolution Rapid Refresh (HRRR), which is running at NCMRWF on an experimental basis consists of Advanced Research Weather Research to forecast the atmospheric fields and - Gridpoint Statistical Interpolation (WRF-GSI) for creating the assimilated initial fields. It is a state-of-the-art, convection-allowing, storm-resolving, real-time, hourly updated model system that provides short-range (lead time ranges upto 24 h) high-resolution (horizontal resolution 1.5 km with 80 vertical levels) forecasts over East India region (Fig.1). The region of interest is used to impact by heavy rainfall, lightning, and strong winds caused by frequent convective systems. HRRR setup over this region is designed to monitor the high-impact weather events during the summer season.

## 2. Experimental setup

The details of the physical parameterization options employed in HRRR system is shown in Table 1a. The model is initialized with IMD-GFS T1534 and lateral boundary conditions are updated 3 hourly and the conventional, satellite radiances, radar and lightning flashes are being assimilated hourly (Table 1b). Model initial fields are generated using the GSI based 3DVAR technique. The GSI cloud analysis package is used to convert the lightning flash counts into proxy reflectivity. Both the radar reflectivity and proxy reflectivity calculated from lightning flash counts are converted to latent heat temperature tendencies (LHT) and it replaces the model-derived 3D LHTs. These estimated LHT profiles are substituted to the WRF microphysics scheme during the Digital Filter Initialization (DFI) forward step at every 15 min (Benjamin et al., 2016), which forces the model to initiate convection during the pre-forecast period. For a model column to be categorized as a convective region, the maximum temperature tendency must be more than 0.0002 K/s. To evaluate the importance of high resolution and rapid update, two experiments have been conducted on 31 Mar 2023 heavy rainfall case (i) Control (CNTL) without any data assimilation and (ii) HRRR with hourly assimilation of observations (both conventional and satellite radiances along with the radar and lightning). To evaluate different facets of the forecast quality, a variety of verification metrics like Probability of Detection (POD), False Alarm Ratio (FAR), Threat Score (TS) are used.

## 3. Results and Discussion

The spatial distribution of rainfall from model experiments (CNTL and HRRR) is compared with NCMRWF-IMD merged rainfall (Fig. 2). The observed rainfall system over Odisha is well captured by HRRR though there are some over-estimations in the amount. The spatial spread of the rainfall system is poorly represented in CNTL. This is reflected in the evaluation metrics. HRRR provides a large POD (0.8), ETS (0.4) and TS (0.7) whereas CNTL shows lower scores. FAR is comparably lesser in CNTL (0.1) than HRRR (0.2), but which is acceptable in the case of HRRR while considering the other scores. It is concluded that rapidly updated hourly assimilation is able to simulate the heavy rainfall event well.

## References:

- Benjamin, S. G., Weygandt, S. S., Brown, J. M., Hu, M., Alexander, C. R., Smirnova, T. G., Olson, J. B., James, E. P., Dowell, D. C., Grell, G. A., Lin, H., Peckham, S. E., Smith, T. L., Moninger, W. R., Kenyon, J. S., & Manikin, G. S. (2016). A North American hourly assimilation and model forecast cycle: The rapid refresh. *Monthly Weather Review*, 144(4), 1669–1694. <https://doi.org/10.1175/MWR-D-15-0242.1>
- Kong, R., Xue, M., & Liu, C. (2018). Development of a Hybrid En3DVar Data Assimilation System and Comparisons with 3DVar and EnKF for Radar Data Assimilation with Observing System Simulation Experiments. *Monthly Weather Review*, 146(1), 175–198. <https://doi.org/10.1175/MWR-D-17-0164.1>

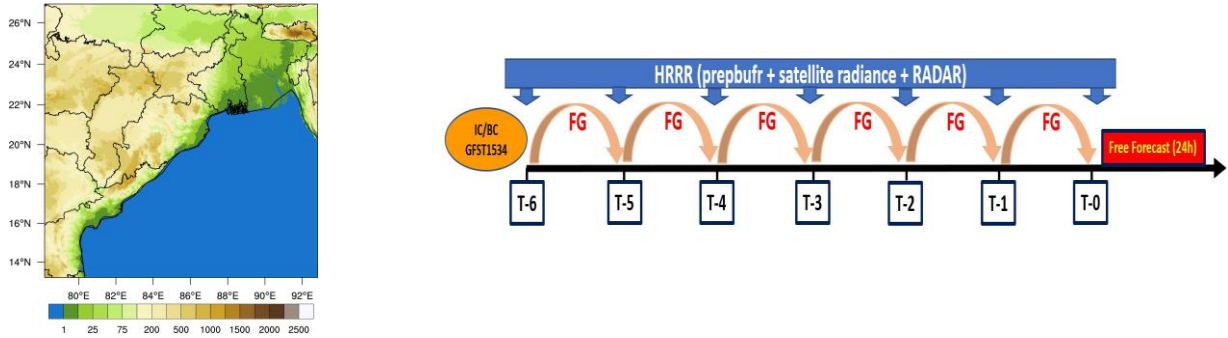


**Fig. 1** (a) Study area with a resolution of 1.5 km (Topography of the domain in shading), (b) Schematic of HRRR assimilation and forecast system

**Table 1.** Model Physics Configuration and Assimilated Observations in HRRR

WRFV 3.9.1		Conventional		Satellite Radiance	
Horizontal resolution	1.5 km	Radiosondes	SSMIS: F17, F18		
Vertical levels	80	Pilot Balloon	HIRS: N19, MetOp-B		
Time step	6 seconds	Aircraft observations	AMSU-A: N15, N18, N19, MetOp-B, MetOp-C		
Output frequency	1 hour	Satellite AMVs	INSAT 3DR		
Grid points	1050 x 1050 (13.19°N to 26.9 1°N) (78.17°E to 92.83°E)	Scatterometer	ATMS: n20		
<b>Physical Parameterization Schemes</b>		Radar radial winds	IASI: MetOp-B		
Radiation	RRTMG for both short and long wave radiation	GPSRO	MHS: N19, MetOp-B & C		
Boundary layer	MYNN-EDMF scheme		ATMS: NPP, N20		
Microphysics	Morrison scheme		AVHRR: N19		
Cumulus Convection	Turned off		SEVIRI Clear-sky		
Land surface	Noah Land surface scheme		AHI		

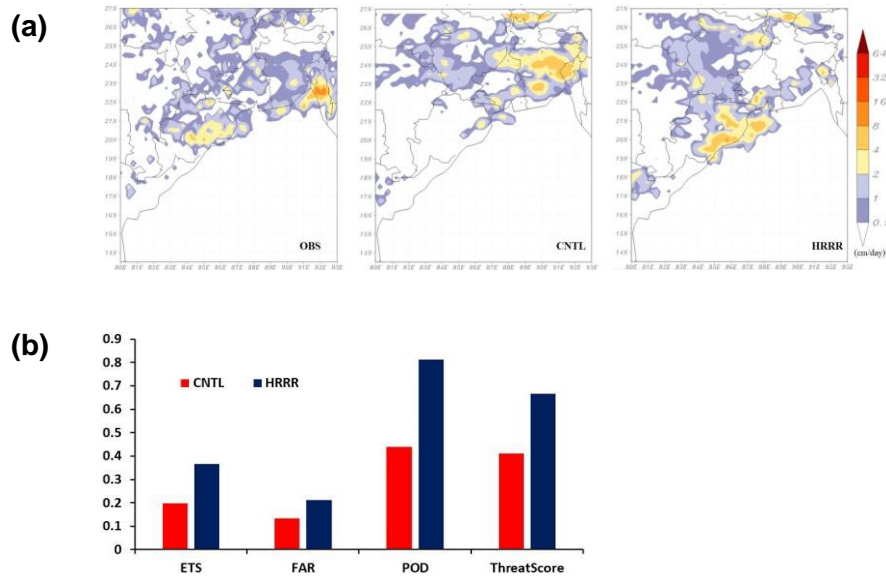


**Fig. 2.** Spatial distribution of 24 hour accumulated rainfall (cm/day) for the event 31 Mar 2023 from (a) satellite - gauge merged rainfall (NCMRWF-IMD), (b) Verification metrics from CNTL and HRRR experiments

# Operational use of Dual-Metop AMVs at high latitudes in JMA's global NWP system

NONAKA Kenichi

Numerical Prediction Development Center, Japan Meteorological Agency

E-mail: k-nonaka@met.kishou.go.jp

## 1. Introduction

JMA's global numerical weather prediction (NWP) system involves the use of assimilated atmospheric motion vectors (AMVs) generated from geostationary (GEO) and low-earth-orbiting (LEO) satellite imagery. GEO AMVs are available for the area between around 60°S and 60°N, while LEO and LEO-GEO AMVs are used in analysis by the system for high latitude region (Yamashita 2014). LEO AMVs from sources such as MODIS and AVHRR, are derived from sequential single LEO satellite images scanned over polar regions, where there is an overlap. LEO-GEO AMVs are derived from GEO/LEO synthetic imagery by the Cooperative Institute for Meteorological Satellite Studies (CIMSS), covering high latitude bands (50 – 70° north and south), where there is a coverage gap between GEO and LEO AMVs (Lazzara et al. 2014).

Dual-Metop AMVs are an AVHRR wind product provided by the European Organisation for the Exploitation of Meteorological Satellites (EUMETSAT) (Hautecoeur and Borde 2017). These are derived from two sequential AVHRR images of tandem Metop-B and -C, with coverage of the globe including both poles. Images are scanned approximately 50 minutes apart, which is shorter than the periodicity of single AVHRR AMVs (approx. 100 min). There are more vectors and less acquisition latency due to the use of these higher temporal resolution images, providing advantages in use of the data in NWP systems.

Against this background, JMA explored the use of Dual-Metop AMVs to supplement high-latitude coverage of global analysis. This report outlines quality control for assimilation of the new data and its effects on forecast fields of observing system experiments (OSEs) in the global NWP system.

## 2. Dual-Metop AMVs

In JMA's global NWP system, cycle analysis and early analysis are operated on a six-hourly basis. Early analysis is performed for operational forecasting with shorter cut-off times (2 hrs at 00, 06, 12 and 18 UTC) than cycle analysis (12 hrs at 00 and 12 UTC and 8 hrs at 06 and 18 UTC). Figure 1 shows an example of the northern polar AMV distribution used in cycle analysis (left) and early analysis (right).

Dual-Metop AMVs dominate coverage around the Arctic Ocean in early analysis because the acquisition time is shorter than that of LEO AMVs.

Dual-Metop AMVs are provided with quality indexes (QI) attached to each vector (Holmlund 1998), both with and without forecast checking. While standard AMV products and related QIs are calculated from three sequential images, Dual-Metop AMVs and related QI calculation are generated from two.

In this context, JMA researched the use of Dual-Metop AMVs with QI at high latitudes including polar areas (poleward from 50° north and south) in global analysis.

## 3. Dual-Metop AMV quality control

In this work, Dual-Metop AMV quality was statistically evaluated against global NWP forecast first-guess values. QIs with forecast checking (QIF) were used to screen out low-quality vectors, as it was found that observation values minus the first-guess (O-B) tended to decrease with QIF values. Figures 2 (a) and (b) show O-B zonal means of Dual-Metop AMV u-components without QIF screening for periods of around a month in summer 2019 and winter 2020, respectively. Figures 2 (c) and (d) are as per (a) and (b), but with large (> 85) QIF vectors. (a) and (b) show significant biases, especially in the upper troposphere (negative bias) and the lower layer (positive bias). (c) and (d) show that QIF screening effectively reduces these biases.

As biases above 300 hPa and below 700 hPa over land were observed even after QIF screening, Dual-Metop AMVs at these heights were set to not be used in global analysis.

## 4. OSEs and summary

OSEs were conducted to assess Dual-Metop AMV effects on global NWP based on JMA's operational system as of September 2020. Assuming that the LEO AMVs used in analysis to date would become unavailable due to the retirement of legacy satellites (such as Terra and Aqua), control experiments (CNTL) were performed without the use of polar MODIS and AVHRR AMVs to determine the effects of assimilating only the new data. Test experiments (TEST) were also run with the

Dual-Metop AMVs used in CNTL. The OSEs were for August 2019 and January 2020.

Figure 3 shows zonal means of relative improvement in root mean square errors (RMSEs) of u-component wind and geopotential height for 48-hour forecasts against own analysis (12 UTC initial). Errors in forecast fields for the troposphere are significantly mitigated in TEST at high latitudes in the Northern and Southern Hemispheres in summer and winter.

Dual-Metop AMVs have been operationally used over high-latitude regions in the global NWP system since 30 June 2022.

### References

- Hautecoeur, O., and R. Borde, 2017: Derivation of Wind Vectors from AVHRR/MetOp at EUMETSAT, *J. Atmos. Oceanic Technol.*, **34**, 1645-1659
- Holmlund, K., 1998: The utilization of statistical properties of satellite-derived atmospheric motion vectors to derive quality indicators, *Wea Forecasting*, **13**, 1093-1104
- Lazzara, M. A., R. Dworak, D. A. Santek, B. T. Hoover, C. S. Velden, and J. R. Key, 2014: High-Latitude Atmospheric Motion Vectors from Composite Satellite Data, *J. Appl. Meteor. Climat.*, **53**, 534-547
- Yamashita, K., 2014: Introduction of LEO-GEO and AVHRR Polar Atmospheric Motion Vectors into JMA's Operational Global NWP System, *CAS/JSC WGN Res. Act. Atmos. Ocea. Model.*, **11**, 1-25

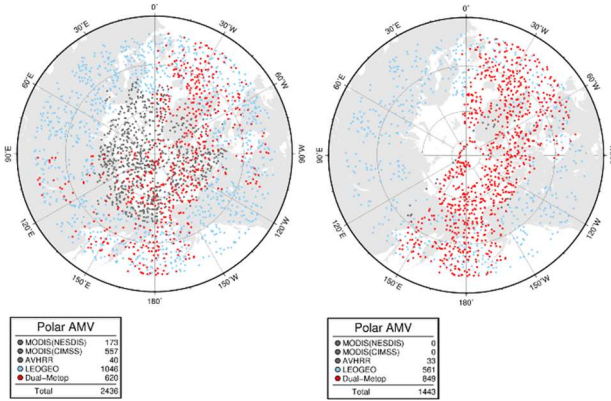


Figure 1: North polar AMVs used in global analysis for 00 UTC on 1 Jul. 2020. Points indicate Dual-Metop (red), MODIS (grey) and LEO-GEO (light blue) AMVs. Left and right are polar AMVs used in cycle analysis and early analysis, respectively.

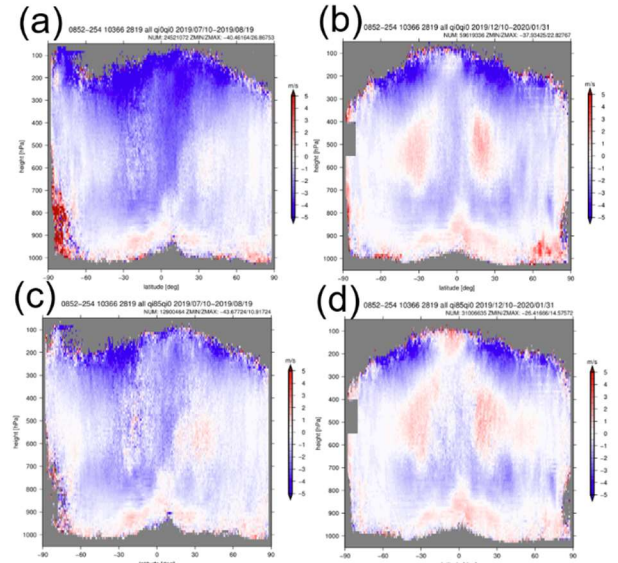


Figure 2: Zonal means of u-component wind differences between Dual-Metop AMVs and first guess (O-B) [m/s]. a/b: without QIF screening; c/d: with large QIF values (> 85). Left and right are for 10 Jul. – 19 Aug. 2019 and 10 Dec. 2019 – 31 Jan. 2020, respectively. The horizontal and vertical axes indicate latitude [deg.] and pressure [hPa], respectively.

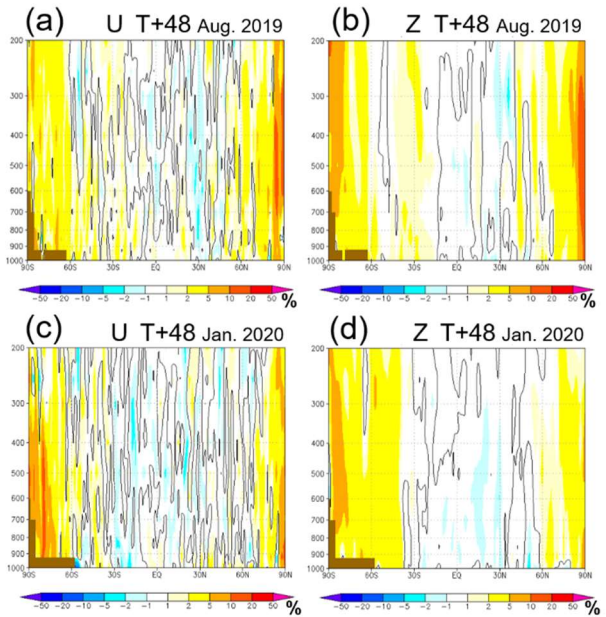


Figure 3: Zonal means of relative improvement [%] in terms of root mean square error (RMSE) with u-component wind and geopotential height for 48-hour forecasts from a 12 UTC initial against own analysis. a/b: Aug. 2019; c/d: Jan. 2020. The horizontal and vertical axes indicate latitude [deg.] and pressure [hPa], respectively. Warm colors indicate improved TEST results over CNTL.

# Inserting Intermediate Generations in a Multigrid Beta Filter using Offset Diagonal Grids and Characterizing the Analysis Error

R. James Purser, Miodrag Rancic, and Manuel Pondeca  
Lynker at NOAA/NCEP/EMC  
Email: jim.purser@noaa.gov

## 1. Multigrid beta filter

The multigrid beta filter (MGBF) is being developed at NOAA’s Environmental Modeling Center as a method for simulating the covariance operators used in data analysis or assimilation. It is expected initially to replace the recursive filter (Wu et al.) covariance scheme in the Real-Time Mesoscale Analysis (RTMA, see de Pondeca et al. 2011) on a limited-area rectangular domain, but a version is also being developed for the global domain using gnomonic cubed-sphere grids, each similar to the one used by the global FV3 model, but in a hierarchy of successively coarser scales for simultaneous parallel processing of additive quasi-Gaussian contributions to the final covariance. The advantage of the MGBF scheme over the recursive filter scheme is that it is capable of being made highly parallelizable since each of the quasi-Gaussian contributions are of finite support (unlike the recursive filters), which leads to relatively simple spatial decompositions into subdomains that can be handled on separate processors at the same time.

## 2. Diagonal offset grids

We are looking at ways to enhance the versatility of the MGBF scheme by introducing intermediate diagonally aligned horizontal grids in the multigrid hierarchy. In the basic hierarchy of “filtering grids” (on which we apply the quasi-Gaussian beta filters themselves), the progression of successively coarser grids involves a horizontal scale change of exactly two at each step up the hierarchy. Since the horizontal grids are square in the limited domain and on the cubed sphere, it is possible in both cases to expand the hierarchy by interleaving a series of diagonal grids that reduce this jump in scale to a smaller factor of  $\sqrt{2}$ , and thereby expand the range of covariance profile shapes that a judiciously weighted hierarchy of the quasi-Gaussians at each scale can simulate.

If we arrange for the grid points in each subdomain to be offset a half grid space from its boundaries, then the grid-to-grid interpolations down the multigrid hierarchy are achieved with only simple line interpolations, as Fig. 1 shows. Moreover, by carrying auxiliary points in the form of L-shaped quartets just outside each side of each subdomain corner, we avoid the need for any further halo exchanges as this procedure proceeds down the hierarchy of scales (or, in its adjoint version, up the hierarchy).

## 3. Estimating analysis error

We propose to approach the difficult problem of estimating the analysis error by employing the beta filter itself to first smooth the precision-weighted distribution of

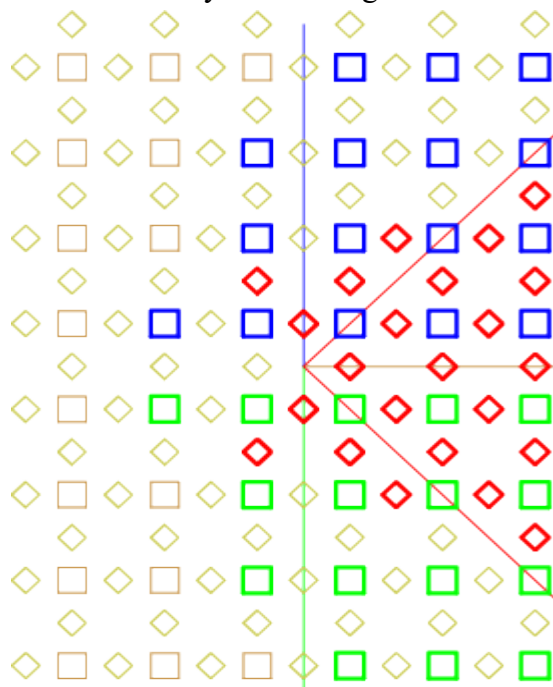


Fig.1: Arrangement near the corner of subdomains showing how interpolation from the coarser offset grid to the finer one, diagonally oriented to it, can be accomplished by 4-point interpolation along lines. When the L-shaped quartets of auxiliary grid values on both sides of each subdomain corner are appended, it is possible to carry out these interpolations without recourse to further lateral exchanges of data at each step in the hierarchy of grid-to-grid interpolations.

unit impulses at each observation location to obtain a precision-weighted data density. The filter in this case can be a single quasi-Gaussian at a relatively coarse scale taken from the multigrid formulation. Then, since at each grid point, we know the superposition weights used to characterize the background error covariance, and knowing the quasi-Gaussian form of the filters they are applied to, it is possible to perform a local virtual “analysis” in the Fourier domain that assumes homogeneity of both background covariance, and observation density and to extract a corresponding local spectral representation of the analysis error’s spectrum – in effect, a power spectrum of the expected error in the local analysis. This can be projected onto the given space of the local multigrid scale weights to provide a fairly informative characterization of the spatial form of the expected analysis error, or we can simply extract the variance part of this calculation at each point. In this way, we should be able to use the machinery of the multigrid beta filter itself to extract from the given distribution of the data, and its known errors, a fair characterization of the optimal analysis error, which would otherwise be difficult to estimate.

## References

- De Ponca, M. S., and Coauthors, 2011: The Real-Time Mesoscale Analysis at NOAA’s National Centers for Environmental Prediction: Current status and development. *Wea. Forecasting*, **26**, 593–612.
- Purser, R. J., M. Rančić, M.S.F.V. De Ponca, 2022: The Multigrid Beta function approach for modeling of background error covariance in the Real-Time Mesoscale Analysis (RTMA), *Mon. Wea. Rev.*, **150**, 715–732. <https://doi.org/10.1175/MWR-D-20-0405.1>
- Wu, W.-S., R. J. Purser, and D. F. Parrish, 2002: Three-dimensional variational analysis with spatially inhomogeneous covariances. *Mon. Wea. Rev.*, **130**, 2905–2914.

# Calibration of the Multigrid Beta Filter for Application in GSI and JEDI

Miodrag Rancic<sup>1</sup>, R. James Purser<sup>1</sup>, Manuel De Ponca<sup>1</sup>, Ting Lei<sup>1</sup>, Sho Yokota<sup>2</sup>

<sup>1</sup>Lynker at NOAA/NCEP/EMC

<sup>2</sup>NCEP Visiting Scientist on leave from the Japan Meteorological Agency

Email: Miodrag.Rancic@noaa.gov

The Multigrid Beta Filter (MGBF), an efficient and scalable covariance operator, is being incorporated in the data assimilation systems used at NOAA's Modeling Center, the Grid-point Statistical Interpolation (GSI) and Joint Effort for Data Assimilation (JEDI), where it will replace the Recursive Filter (RF) (e.g., see Purser et al. 2003 for an isotropic application in GSI). On massively parallel computers, the computational domain is decomposed and parallelized horizontally. For that reason, a sequential operator, such as a RF, though by itself is very efficient, has difficulties exploiting computational parallelism in modeling horizontal covariances with large horizontal spread over several computational domains. The MGBF technique, which solves this problem by application of a Beta filter with a compact support applied through a multigrid paradigm, demonstrated a superior scaling in all preliminary tests (e.g., Purser et al., 2022, Rancic et al., 2023).

Performance of the MGBF in the homogeneous and isotropic case that we consider for now depends on several parameters. The main version of the filter, which applies the 2D version of the beta radial filter horizontally, followed by a swipe of a 1D beta filter applied in vertical directions, relies on parameters of the horizontal and vertical aspect tensors (in the isotropic version only their intensities,  $a_h$  and  $a_v$ ), and scale weights applied to each multigrid generation  $w_i, i = 1, 2, \dots, n$ , where  $nn$  is the number of generations. Thus, this set of parameters needs to be predefined for a successful performance of the filter. We use error statistics generated by the NMC method as a reference for calibration, from which we get typical horizontal and vertical correlation lengths ( $\lambda_h, \lambda_v$ ) for the various atmospheric fields. Technically, the task of calibration is to find multigrid parameters:

$$a_h, a_v, w_i = f(\lambda_h, \lambda_v)$$

Clearly, this problem does not have a unique solution. Thus, for now we adopted an approach which, though it does not guarantee the best combination of parameters, provides a set that will lead to normalized covariances of the required size in all directions. To this end, we assume a preliminary set a scale weights which gives a reasonable height of the resulting covariances, and then run a series of tests in a standalone version of the MGBF code in which we prescribe forcing by a unit impulse and vary only intensities of aspect tensors. On the output, we measure the amplitude of the resulting covariance,  $\psi_{max}$ , and the resulting correlation lengths, ( $l_h, l_v$ ). In such a constellation, the derived correlation lengths are only functions of the intensities of aspect tensors,  $a_h$  and  $a_v$ . When the initial predefined set of scale weights is divided by the maximum of the resulting covariance,  $\psi_{max}$ , in a repeated test we derive a normalized covariance of the same size. This method is for now applied in a tabular fashion, where input correlation lengths from the NMC method, ( $\lambda_h, \lambda_v$ ), are compared with the normalized covariances of the length ( $l_h, l_v$ ), produced by the MGBF in standalone tests, in order find correct values of aspect tensors ( $a_h, a_v$ ) that need to be used in GSI. In future, we plan to apply a machine learning (ML) version

of this algorithm, in which an artificial neural net (ANN) will be applied instead of lookup tables to accomplish the same task.

Along the way we have found that vertical covariances may have unexpectedly long correlation lengths. To avoid possible issues with the efficiency which that could cause, we have developed a new flavor of the MGBF, in which the multigrid logistics is applied not only in the horizontal, but both in horizontal and vertical directions, as schematically illustrated in Fig. 1. Technically, we consistently reduce vertical resolution at each successive grid generation, which systematically eliminates the need for large vertical filter swapes, in terms of number of grid spaces, at generations with higher resolutions.

Initially, MGBF was developed having in mind only modeling of the background error. However, new possible applications are emerging (e.g., localization of ensemble, analysis error, scale selection, etc.). Thus, an object-oriented version of the MGBF code is being developed, which is primary targeting application in the framework of the new data assimilation system, JEDI.



**Fig. 1.** On the left, schematically presented standard MGBF paradigm, in which vertical resolutions of all grid generations are treated equally. On the right, the latest MGBF version, in which vertical resolutions of successive grid generations are systematically reduced (halved). The thick grid boxes represent processors; G1, G2, and G3 denote successive grid generations 1, 2 and 3.

## References

- Purser, R. J., W.-S. Wu, D., F. Parrish, and N. M. Roberts, 2003: Numerical aspects of the application of recursive filters to variational statistical analysis. Part I: Spatially homogeneous and isotropic Gaussian covariances. *Mon. Wea. Rev.*, **131**, 1524–1535.
- Purser, R. J., M. Rancic, M.S.F.V. De Ponca, 2022: The Multigrid Beta function approach for modeling of background error covariance in the Real Time Mesoscale Analysis (RTMA), *Mon. Wea. Rev.*, **150**, 715-732. <https://doi.org/10.1175/MWR-D-20-0405.1>
- Rancic, M., R. J. Purser, M. Ponca, E. Colon, T. Lei, and S. Yokota, 2023: 27IOAS Multigrid Beta Filter Covariance Operator: Latest Updates of the Technique and Parallel Runs in 3D RTMA, 7A.2. *103<sup>rd</sup> Annual Meeting of American Meteorological Society, Denver, CO & Online, 8-12 January 20*

## Satellite Microwave instruments in the low earth inclined orbits for NWP: Contribution from India

S. Indira Rani, V. S. Prasad and John P. George  
National Centre for Medium Range Weather Forecasting (NCMRWF)  
Ministry of Earth Sciences (MoES),  
A-50, Institutional Area, Sector-62, Noida-201301, U.P. India  
[indirarani.s@gov.in](mailto:indirarani.s@gov.in), [indira@ncmrwf.gov.in](mailto:indira@ncmrwf.gov.in)

Megha-Tropiques (MT) was a joint Indo-French Satellite mission launched by the Indian Space Research Organization (ISRO) on 12 October 2011. MT was positioned in a highly inclined equatorial plane of  $20^\circ$  at a height of 867 km above the Earth so as to orbit the tropical region between  $30^\circ\text{N}$  and  $30^\circ\text{S}$  nearly 14-15 times a day. There were four payloads onboard MT, consisting of a Microwave radiometer (MADRAS), a microwave humidity sounder (SAPHIR), a radiation budget instrument (SCARAB) and a radio occultation sounder (ROSA). SAPHIR was one of the highly used microwave humidity sounder observations by the leading global operational NWP centres (Chambon et al., 2015, Chambon and Geer, 2017, Singh and Prasad, 2017, Jones et al., 2017, Doherty et al., 2018, Kumar et al. 2018).

A collaborative study between NCMRWF and the UK Met Office reported the NWP requirement of microwave imager and sounder together in the same satellite platform and demonstrated that the humidity sounders ATMS, MHS, and SAPHIR perform similarly; however SAPHIR notably outperforms the other instruments between 650 and 1000 hPa (Doherty et al., 2018). This is due to the lowest peaking channel of SAPHIR ( $183.31 \pm 11$  GHz) which is absent in both ATMS and MHS. Since the MADRAS onboard MT was not functional, the performance of AMSR-2 and SAPHIR and their combined impact showed that the imager (AMSR-2) assimilation produces lowest errors in specific humidity below 600 hPa, while SAPHIR performs best at higher altitudes (Rani et al., 2016).

MT was decommissioned in January 2022. On 10 February 2023, ISRO launched a follow-on experimental mission (Microsat-2B) to SAPHIR in a low earth circular orbit of  $37^\circ$  inclination at an altitude of 450 km above the Earth, with an expected life period of 12 months. This mission is also known as Earth Observation Satellite seven in the series (EOS-07). Table-1 shows the specifications of EOS-07 and MT-SAPHIR. There are slight differences in the channels frequencies of SAPHIR and Microsat-2B. The channel frequencies are slightly shifted down in Microsat-2B compared to SAPPHIR. Figure 1 shows the weighting functions of SAPHIR and Microsat-2B humidity sounder channels over a tropical location. It is expected that the NWP centres will benefit from the EOS-07 mission also.

Table 1: Satellite parameters of EOS-07 and Megha-Tropiques

Parameter	Specifications	
	EOS-07	Megha-Tropiques (SAPHIR)
Launch date	10 February 2023	12 October 2011
Orbit	Circular, $37^\circ$ inclination	Drifting, $20^\circ$ inclination
Altitude	450 km	867 km
Swath	1050 km	1700 km
Frequency Band	183.31 GHz	183.31 GHz
Spatial resolution Nadir	10 km	10 km
Mission Life	12 months	10 years (2011-2022)

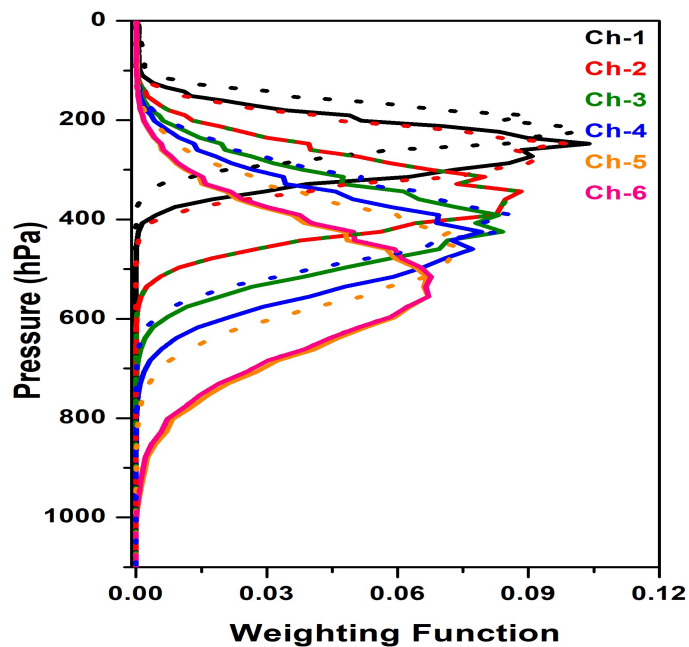


Figure 1: Weighting functions of SAPHIR (dotted) and Microsat-2B (continuous) humidity channels over a tropical location.

#### References

A. Doherty, S. Indira Rani, Stuart Newman, William Bell., "Benefits of Assimilating SAPHIR Observations on Analysis and Forecasts of Tropical Fields in the Met Office Global Model", *Q J R Meteorol Soc.*, 2018, <https://doi.org/10.1002/qj.3258>

E.E. Jones, K. Garrett, S.A. Boukabara, Assimilation of Megha-Tropiques SAPHIR observations in the NOAA global model, *Mon. Weather Rev.*, 145 (2017), pp. 3725-3744, 10.1175/MWR-D-16-0148.1

P. Chambon, A.J. Geer , All-Sky Assimilation of Megha-Tropiques/SAPHIR Radiances in the ECMWF Numerical Weather Prediction System, European Centre for Medium-Range Weather Forecasts (2017), Technical Memo

P. Chambon, L.F. Meunier, F. Guillaume, J.M. Piriou, R. Roca, J.F. Mahfouf, Investigating the impact of the water-vapour sounding observations from SAPHIR on board Megha-Tropiques for the ARPEGE global model, *Q. J. R. Meteorol. Soc.*, 141 (2015), pp. 1769-1779, 10.1002/qj.2478

S. I. Rani, Amy Doherty, Nigel Atkinson, William Bell, Stuart Newman, Richard Renshaw, John P. George, and E. N. Rajagopal 2016: " Effect of new radiance observations on numerical weather prediction models ", *Spie Newsroom*, 10.1117/2.1201607.006533 Page 4/4.

S. K. Singh and V. S. Prasad, Impact of Megha-Tropiques SAPHIR radiances in T574L64 global data assimilation and forecasting system at NCMRWF, *International Journal of Remote Sensing* (2017), 38:16, 4587-4610, DOI: [10.1080/01431161.2017.1323279](https://doi.org/10.1080/01431161.2017.1323279)

S. Kumar, S. Indira Rani, John P. George, E. N. Rajagopal., "Megha-tropiques SAPHIR radiances in a hybrid 4D-Var data assimilation system: Study of forecast impact", *Q J R Meteorol Soc.*, 2018, <https://doi.org/10.1002/qj.3251>.

# High Resolution Rapid Refresh Data Assimilation System at NCMRWF (India) for Convection Permitting Models

Ashish Routray\*, Devajyoti Dutta, John P. George and V. S. Prasad

National Centre for Medium Range Weather Forecasting (NCMRWF), Ministry of Earth Sciences (MoES), A-50,  
Sector-62, Noida UP-201309, India

E-mail address: [ashishroutray.iitd@gmail.com](mailto:ashishroutray.iitd@gmail.com); [ashishroutray@ncmrwf.gov.in](mailto:ashishroutray@ncmrwf.gov.in)

## 1. Introduction:

High impact convective weather events evolved with different microphysical and dynamical processes that operate at very small horizontal and time scales. To resolve their properties, the high resolution mesoscale models must be configured with horizontal resolution about 1 to 2 km as well as increase of frequency of assimilation cyclic. In recent years, the high temporal and spatial resolution observational data like Doppler Weather Radar (DWR) are available. Given the need for more accurate prediction of high impact weather systems in short-time scale, the High-Resolution Rapid Refresh (HRRR) Data Assimilation (DA) system for the convection permitting models is required.

The National Centre for Medium Range Weather Forecasting (NCMRWF) has set up a HRRR DA system with regional NCUM-R forecast model. Hourly updating HRRR system for the 1.5 km resolution convection permitting NCUM-R has been configured for three specific domains over the Indian region (Fig-1a; Routray et al. 2022). Indian Doppler Weather Radar (DWR) reflectivity observations from various locations are included in the HRRR data assimilation system. The high resolution four dimensional variational (4DVAR) analyses system is used to assimilate DWR radial velocity and reflectivity along with other observations (Dutta et al. 2019) in HRRR assimilation cyclic. The schematic diagram of the hourly HRRR assimilation cycle is given in Fig-1b. The lateral boundary conditions for the forecast model are obtained from Indian domain 4 km resolution operational NCUM-R. To assess the beneficial impact of 1hrly updated HRRR DA system a case study during convective event (7<sup>th</sup> June 2021) is presented here (Domain-2 in Fig-1a). Two setup numerical experiments such as CTL (without assimilation) and HRR (1hrly assimilation of DWR observations along with others) are presented. The assimilation cycle is started 6 hrs before from the model integration (Fig-1b).

## 2. Result of the case study:

The 24 hrs accumulated model simulated (day-1) and observed rainfall are shown in Fig-2(a-e). The observed rainfall clearly shows wide spread heavy rainfall about 8-16 cm around the vicinity of Agartala DWR (Fig-2a). From the CTL simulation (Fig-2d), the simulated heavy rainfall patches are shifted more northeast wards and not able to simulate the heavy rainfall over the eastern part of Agartala. However, the HRR (Fig-2e) is able to reproduce the orientation, pattern and volume of rainfall in better way than the CTL simulation. These features are reasonably well correlated with the observations. From Fig-2f, the ETS values are relatively high in the HRR experiment in all thresholds as compared to the CTL. It is clearly deduced that the high intensity of rainfall is well simulated by the HRR experiment than the CTL experiment. The gain of improvement is comparatively high in the higher threshold of rainfall (> 50mm) in HRR with respect to the CTL. Figure-3 shows various statistical skill scores of rainfall obtained through Contiguous Rain Area (CRA) method. The figure clearly depicts that the statistical skill scores are better represented in the HRR than the CTL experiments.

It can be concluded from the present study that the hourly updated cyclic assimilation in the high resolution modeling approach with assimilation of DWR observations has beneficial impact on the simulation of convective weather systems and these systems can be utilized for nowcasting and short range weather forecasting applications.

## References:

- Dowell, D. C., and Coauthors, 2022: The High-Resolution Rapid Refresh (HRRR): An hourly updating convection-allowing forecast model. Part I: Motivation and system description. *Wea. Forecasting*, 37, 1371-1395, <https://doi.org/10.1175/WAF-D-21-0151.1>.
- Dutta, D., Routray, A., Preveen Kumar, D., George, J.P., 2019. Regional Data Assimilation with the NCMRWF Unified Model (NCUM): impact of Doppler Weather Radar Radial Wind. *Pure Appl Geophys*. 176, 4575–4597.
- Routray, A., D. Dutta, K. Amarjyothi, J. P. George and A. K. Mitra., (2022): Radar Reflectivity Assimilation in a Rapid Refresh System for High Resolution NCUM-R, *UM Users Newsletter Issue 23*, March 2022, p-14-16 (<https://info.metoffice.gov.uk/1XRP-7M6U2-A7D10B6DB39886D7WZLD758770223FD64687D6/cr.aspx>).

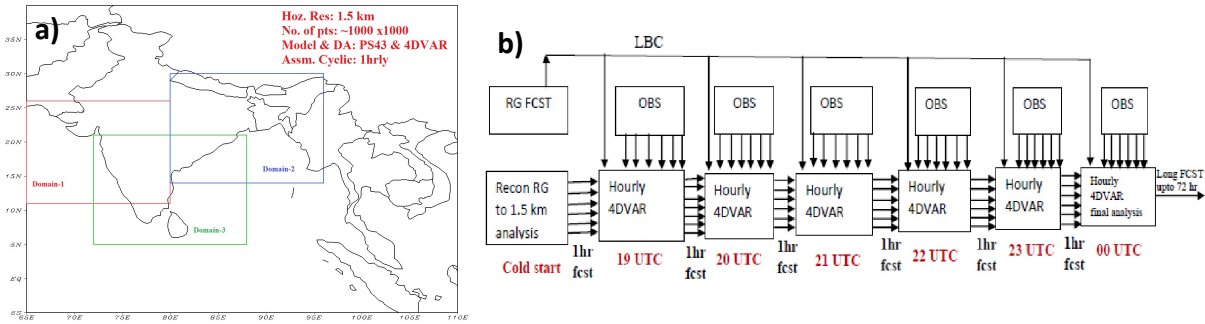


Fig-1: a) Configured different domains for HRRR DA over Indian region and b) Schematic diagram of 1hrly HRRR DA cycle.

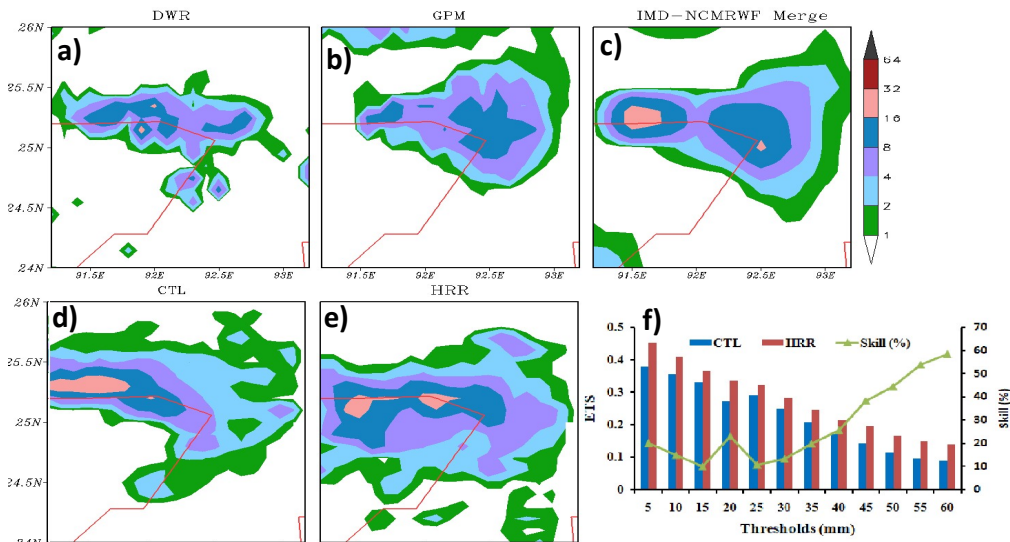


Fig-2: 24 hrs accumulated rainfall from (a) Agartala DWR; (b) GPM satellite; (c) merged satellite-rain gauge analysis (NCMRWF-IMD); (d) CTL; (e) HRR experiment valid at 03 UTC 8 June 2021 and f) ETS along with skill (%; line) of HRR over CTL of day 1 for different thresholds of rainfall (mm).

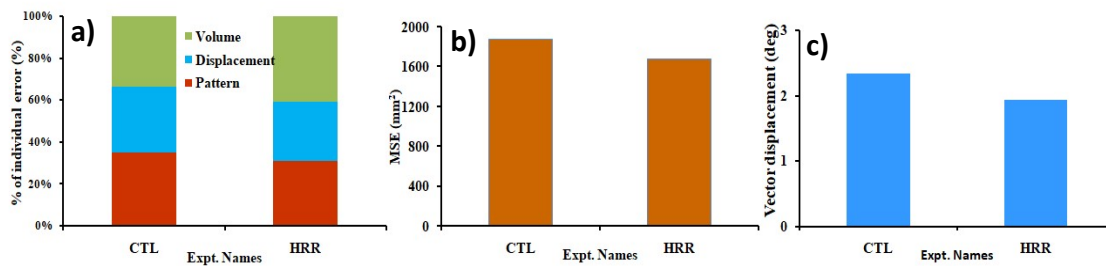


Fig-3: CRA verification of rainfall for threshold 10 mm a) % of contribution of volume, displacement and pattern errors; b) Total Mean Square Error (MSE) and c) vector displacement error (deg.) valid at 00 UTC 08<sup>th</sup> June 2021.

# Soil Moisture Assimilation for Regional NCUM-R Model and its Benefits

Ashish Routray\*, Abhishek Lodh<sup>#</sup>, Devajyoti Dutta, and John P. George

National Centre for Medium Range Weather Forecasting (NCMRWF), Ministry of Earth Sciences (MoES), A-50, Sector-62, Noida UP-201309, India

<sup>#</sup>Current affiliation: Department of Physical Geography and Ecosystem Science, Lund University, Lund, Sweden

\*E-mail address: [ashishroutray.iitd@gmail.com](mailto:ashishroutray.iitd@gmail.com); [ashishroutray@ncmrwf.gov.in](mailto:ashishroutray@ncmrwf.gov.in)

## 1. Introduction:

Recent past, there have been tremendous advancements in high-resolution numerical weather prediction (NWP) as well as Data Assimilation (DA) systems. It is now well known that soil moisture (SM) is a key driver in the exchanges of water and heat fluxes between the ground and the atmosphere and the land surface-atmosphere interaction depends on the land surface characteristics. Therefore, the SM plays a major role in regulating the surface weather parameters, low cloud and rainfall. Indian monsoon region has been recognized as a ‘hot spot’ due to the SM-precipitation coupling (Koster et al., 2004) and became an ideal test bed to study the impacts of the land surface on rainfall associated with convective events like monsoon depression (MD). At National Centre for Medium Range Weather Prediction (NCMRWF), many studies have been conducted to understand the impact of land surface on global and regional NWP. The regional version of the “NCMRWF Unified model” (NCUM-R) is used for high resolution NWP. JULES (Joint UK Land Environment Simulator) is the land surface model coupled with both NCUM global and regional versions.

The simplified extended Kalman Filter (sEKF) based Land Surface Data Assimilation (LSDA) system is used to create land surface SM initial conditions for NCUM-R by assimilating ASCAT SM along with 2m humidity and temperature observations (Lodh et al. 2022; Routray et al. 2023). The schematic workflow providing an overview of the regional sEKF based LSDA currently used for assimilation of SM over the Indian region is depicted in Fig. 1a. Results of the numerical experiments carried out to understand the impact of satellite soil moisture observations is presented briefly to demonstrate the significance of soil moisture initialization, especially with the use of satellite observations. Two numerical experiments, namely CTL (incorporating only screen level observations in LSDA) and ASCAT (assimilating both ASCAT SM and screen level observations in LSDA) are carried out. Identical atmospheric initial condition prepared considering the 4DVAR data assimilation technique is used in both experiments. The MD occurred during the period 15-18 August 2018 is considered in this study. The observed track and associated rainfall activities over the region during the life span of the MD are depicted in Fig. 1b.

## 2. Results

The humidity Jacobians valid at 06 UTC 14 August at all four soil layers (0-10 cm, 10-35cm, 35-100 cm, 100-300 cm) are depicted in Fig-2. It is seen that the humidity Jacobians are positive in all over the regions, suggests the increase SM leads to the increase of the surface level humidity. The high positive Jacobians are noticed in uppermost soil layers and relatively low Jacobians in the deeper layers (de Rosnay et al., 2012). Exceptionally, the high increments are noticed over eastern coast of India in the level 4 soil layer may be the saturation of lower soil layer caused for heavy precipitation during the monsoon season as compared to the other parts of the country. The longitudinally averaged (75–86° E) time-latitude cross-section of rainfall (mm/hr) is depicted in Fig-3. Generally, high precipitation occurred in the south-western quadrant of the MD and the northern part of the MD received light rainfall. The GPM observed rainfall is also showing a similar pattern during our study period. Both simulations well simulated the same features, however, the high magnitude of the rainfall is improved in the ASCAT experiment than the CTL experiment. This high amount of precipitation is missing in the CTL simulation during the period. Overall, this study indicates that the use of ASCAT SM in the preparation of SM initial conditions for the regional NWP system helps to improve the forecast of MD.

## References:

- De Rosnay, P., M. Drusch, D. Vasiljevic, G. Balsamo, C. Albergel, and L. Isaksen. 2012. “A Simplified Extended Kalman Filter for the Global Operational Soil Moisture Analysis at ECMWF.” *Q. J. R. Meteorol. Soc* 139 (674): 1199–1213. doi:10.1002/qj.2023.
- Koster, R.D., Dirmeyer, P.A., Guo, Z., Bonan, G., et al., 2004. Regions of strong coupling between soil moisture and precipitation. *Science* 305 (5687), 1138–1140.
- Lodh, A., A. Routray, D. Dutta, J. P. George, and A. K. Mitra. 2022. “Improving the Prediction of Monsoon Depressions by Assimilating ASCAT Soil Moisture in NCUM-R Modeling System.” *Atmospheric Research* 272: 106130. doi:10.1016/j.atmosres.2022.106130.

Routray, A., Abhishek Lodh, Devajyoti Dutta, John P. George and Ashis K. Mitra, 2023: Influence of ASCAT soil moisture on prediction of track and intensity of landfall tropical cyclones, Int. Jr. of Remot. Sens. 44(1), 341-380.

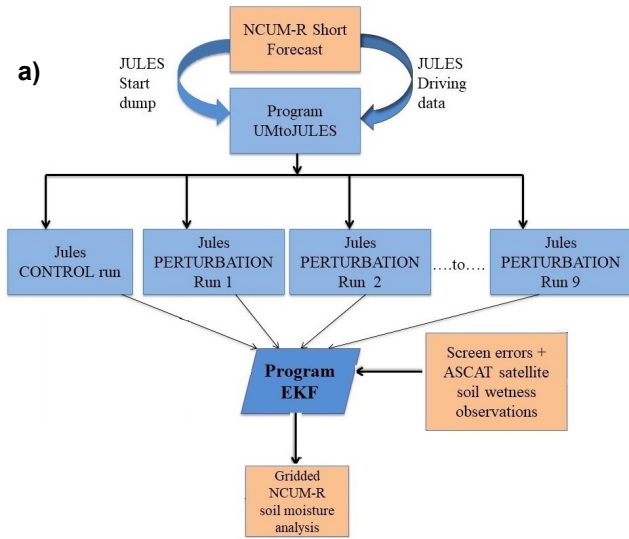


Fig-1a: Schematic of regional sEKF based LSDA

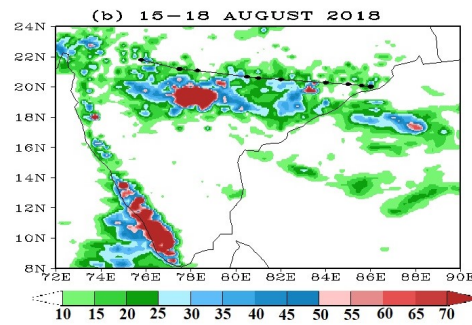


Fig-1b: Time averaged (life span of MD) of IMD-NCMRWF merged rainfall (cm; shaded) and IMD observed track.

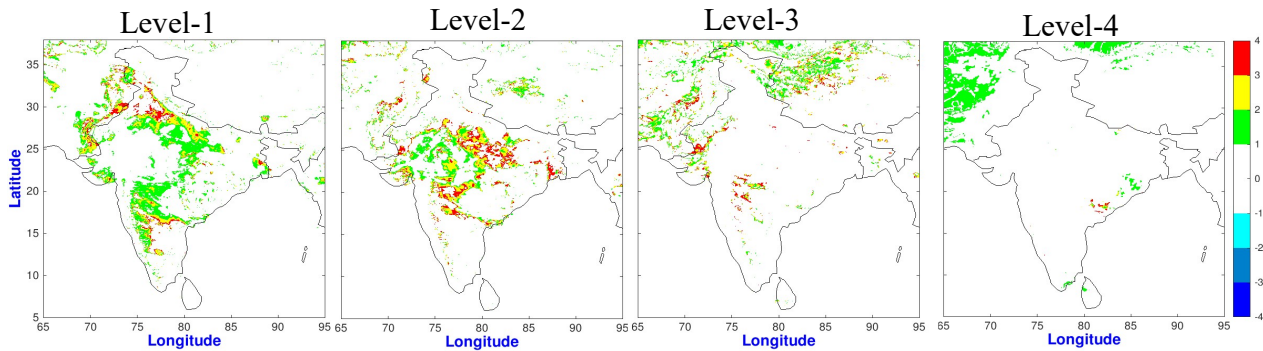


Fig-2: Humidity Jacobians for soil moisture ( $\times 10^{-3} \text{ g/g/m}^3/\text{m}^3$ ) valid at 06 UTC 14 August 2018.

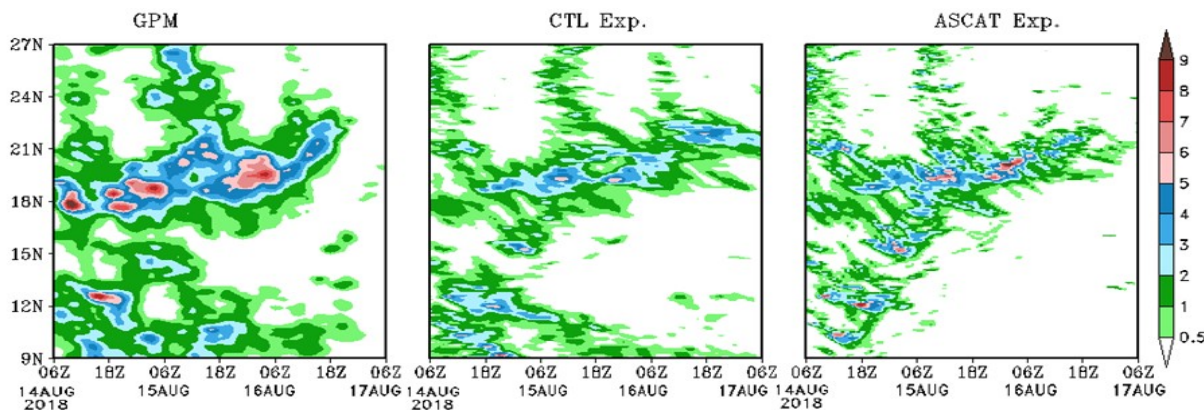


Fig-3: Longitudinally averaged ( $75-86^0 \text{ E}$ ) time-latitude cross section of rainfall (mm/hr)

# Data Assimilation Experiments of Ground-based Microwave Radiometer and small UAV by using Meso-NAPEX

Hiromu Seko, Yasutaka Ikuta, Hiroshi Ishimoto, Kentaro Araki, Tetsu Sakai (Meteorological Research Institute),  
 Kouichi Yoshimoto, Tetsuya Nakamura (Japan Meteorological Agency),  
 Shingo Shimizu (National Research Institute for Earth Science and Disaster Resilience)  
 e-mail:hseko@mri-jma.go.jp

## 1. Introduction

The heavy rainfalls caused by quasi-stationary line-shaped rainfall systems bring about floods or landslides in Japan almost every year. The low-level warm and humid inflow supplied to heavy rainfalls is one of the crucial factors that affect the rainfall amount. To improve the forecast accuracy of quasi-stationary line-shaped rainfall systems, a ground-based microwave radiometer (MWR) network, which observes the precipitable water vapor (PWV), vertical profiles of temperature and humidity, was constructed in western Japan by the Japan Meteorological Agency (JMA) in 2022. Vertical profiles of temperature, humidity, and horizontal wind in the lower atmosphere were observed by a small UAV (unmanned aerial vehicle) aboard a JMA's vessel on the East China Sea (ECS), the upstream side of heavy rainfall, as the part of the intensive observation from June to October 2022 conducted by the Meteorological Research Institute.

These data on low-level inflows to heavy rainfalls are expected to improve the accuracy of numerical forecasts of heavy rainfalls. To show the impact of MWR and small UAV on heavy rainfalls, data assimilation experiments of these observation data were conducted using an experimental system (Meso-NAPEX) based on the operational mesoscale analysis of JMA (Ikuta et al 2021). The results of data assimilation experiments including the observation data of the MWR and small UAV, and their impacts on rainfall forecasts are reported in this paper.

## 2. Assimilation of ground-based MWR

The 14-channel brightness temperatures are obtained by the ground-based MWR every minute. The hourly data of PWV, vertical profiles of temperature and humidity were estimated from the brightness temperatures using the 2-channel method and 1d-var method, respectively (Araki et al 2015). To show their impacts on rainfall forecasts, these data were assimilated in addition to the operationally assimilated data of JMA.

In the assimilation experiments, the MWR data on 11 August 2021 obtained at Fukue in Goto Islands, west of Kyushu, under the second period of the Strategic Innovation Program (SIP2) were used. On that day, a stationary front over Kyushu was moving northward (Fig. 1). During the period of the assimilation window (0 to 3JST 11 August), the observed PWV increased from 45 mm to 55 mm with approaching the front, and the observed PWV was larger than that of first guess by 2-7 mm.

Figure 2 shows 3hour rainfall and the differences in PWVs and wind velocities obtained with and without assimilating the PWV data (wPWV, CTL). By assimilating the PWV data observed by the MWR, the PWV and wind velocity in the ECS, south-western side of Fukue, increased from the first guess at the initial time of forecasts. These increased regions moved northeastward, and then enhanced the rainfall at FT (forecast time) = 3 hours.

As for the vertical profiles obtained by the 1d-var method, the first guess was used in the estimation of vertical profiles and in the assimilation with the Meso-NAPEX. Although it is undesirable using the first guess twice, the 1d-var profiles were assimilated because the information on the vertical profiles is expected to be effective for improving the rainfall forecast. The vertical profiles obtained by the 1d-var show that the low-level inflow below 0.8 km height was more humid and the temperature above 6 km height was colder than those of the first guess (not shown). When the temperature and humidity profiles were assimilated, the amount of water vapor supplied to the rainfall region increased and the atmosphere became more unstable, and then rainfall on the western side of northern Kyushu intensified (wTRH, Fig. 3). When only humidity profiles were assimilated, the rainfalls were weaker than that of TRH (wRH, Fig. 3). This result indicates that the temperature profiles were crucial to increase the accuracy of rainfall amount forecast in this case.

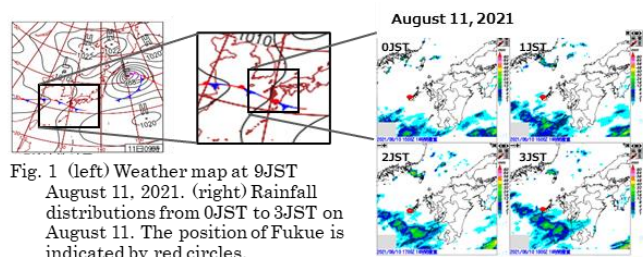


Fig. 1 (left) Weather map at 9JST August 11, 2021. (right) Rainfall distributions from 0JST to 3JST on August 11. The position of Fukue is indicated by red circles.

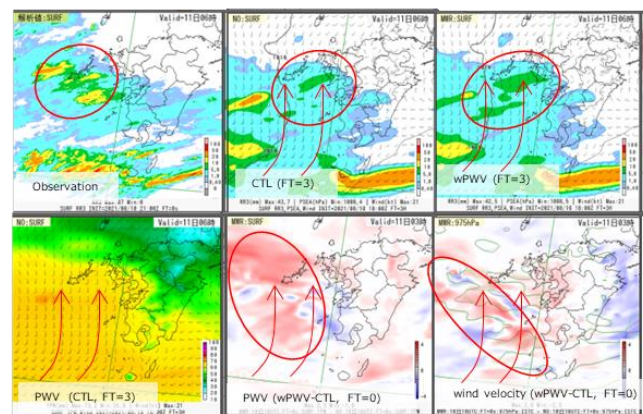


Fig. 2 (top left) Observed 3hour rainfall at 6JST (the same time of FT=3hours). (top center) 3hour rainfall obtained by using only operationally assimilated data of JMA (CTL). (top right) obtained by adding PWV data of MWR to the operationally assimilated data (wPWV). (bottom left) PWV of CTL at FT=3hours. Differences of (bottom center) PWV and (bottom right) wind velocity at FT=0 between wPWV and CTL.

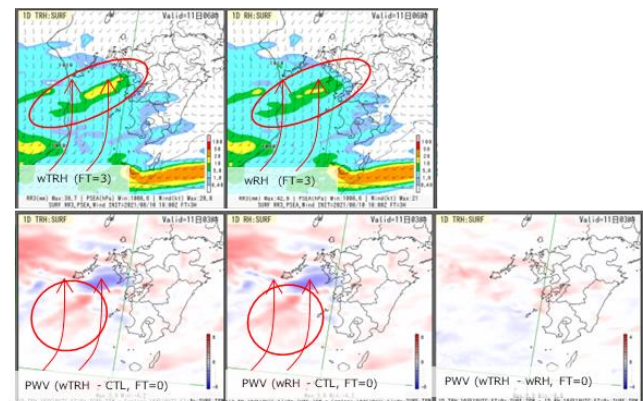


Fig. 3 (top left) 3hour rainfall at FT=3hours obtained by using vertical profiles of temperature and humidity (wTRH). (top center) the same as (top left) but by using vertical profiles of humidity (wRH). Difference of PWV distributions at FT=0 (bottom left) between wTRH and CTL. (bottom center) between wRH and CTL. and (bottom right) between wTRH and wRH.

### 3. Small UAV observation and assimilation result

On 18 July 2022, a heavy rainfall occurred by the stationary front over northern Kyushu (right panel of Fig. 4). From 10 to 12 JST 18 July, the vertical profiles of temperature, humidity, and horizontal wind upstream side of the northern Kyushu in the ECS were obtained by the small UAV aboard the JMA research vessel Ryofu Maru. The maximum heights of observation were 150~300 m because of the strong wind over the sea. The small UAV ascended and descended at the 3 m/s and 2 m/s, respectively. Because the temperature and humidity sensors cannot catch up with the temporal change during the ascent and descent, the observed values were corrected as follows:

$$T_{tru} = T_c + (T_{c+\Delta t} - T_{c-\Delta t})e^{-\frac{2\Delta t}{\tau}},$$

where  $T_c$  is the observed temperature,  $T_{tru}$  is the value after correction,  $\Delta t$  is 30 seconds. As for temperature,  $\tau$  was set to 40 seconds.

The vertical profiles were plotted in Fig. 4. Before the correction, temperatures at the same heights were different between the ascent and descent (top panels of Fig. 5a, blue lines) because the sensor cannot catch up with the temporal change. After the correction, temperature profiles during the ascent and descent were almost the same (orange lines). This result indicates that the correction was successful. Thus, these corrected profiles of temperature were used in the experiments. As for the humidity, the profiles during the ascent and descent differed after the correction, so the averages of the ascent and descent data were used. The horizontal winds during the ascent above 50 m height were used because the anemometer was attached to the upper side of the UAV where less turbulence was expected during the ascent, and the small UAV moved before the ascent to the position where the vessel was expected to be moved while the observation.

Compared with the first guess, the observed temperature was slightly higher, the humidity was larger below 250 m height, and the southerly and westerly winds were more intense during the observation periods. To show the impact of the small UAV data on the forecast more clearly, the one-cycle data of assimilation (10-12 JST 18 July) were added to the operationally assimilated data of JMA in this report. It is expected that the rainfall becomes more intense when these data are assimilated.

When the observation data of the small UAV at the heights of every 50 m from 50 m height were assimilated, PWV and wind speeds increased in the western side of southern Kyushu. Moreover, the area of rainfall over 20 mm increased and be closer to that of the observed rainfall distribution (wUAV, Fig.6). It is found that the small UAV observation can improve rainfall forecasts through data assimilation if it observes the upstream side of the low-level inflow.

### 4. Summary

Assimilation experiments of PWV, vertical profiles of temperature and humidity observed by MWR and temperature, humidity, and horizontal winds in the lower atmosphere observed by small UAV were conducted using Meso-NAPEX. It is found that rainfall forecasts were improved even if the observation data at one point were assimilated, although the impact was weak. To obtain a more conclusive result, it is necessary to increase the number of assimilation data of MWR and small UAV, to assimilate more frequently, and to use brightness temperatures of MWR that include information on the vertical distribution of the temperature and humidity.

### Acknowledgement:

The observation data of MWR at Fukue were provided by the "Second period of Strategic Innovation Program (SIP2)". The assimilation system used in this report was Meso-NAPEX developed by the Numerical Prediction Division, JMA. Small UAV data were obtained by the MRI's project "Research on the mechanism of quasi-stationary line-shaped rainfall systems through intensive observations". The R-SWM (Type-S Co. Ltd., Japan) was used in the small UAV observation. We would like to express our sincere appreciation to the crew of the Ryofu Maru and the staff of the Atmospheric Environment and Ocean Division of JMA for their assistance.

### Reference

- Araki, K., M. Murakami, H. Ishimoto, and T. Tajiri, 2015, Ground-based microwave radiometer variational analysis during no-rain and rain conditions, *SOLA*, **11**, 108-112.  
Ikuta, Y., T. Fujita, Y. Ota, and Y. Honda, 2021, Variational data assimilation system for operational regional models at Japan Meteorological Agency, *J. Meteor. Soc. Japan*, **99**, 1563-1592.

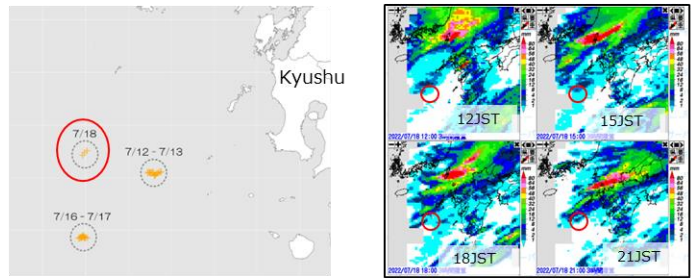


Fig. 4 (left) Positions of small UAV. (right) Rainfall distributions from 12JST to 21JST 18 July 2022. The position of JMA's vessel is indicated by red circles.

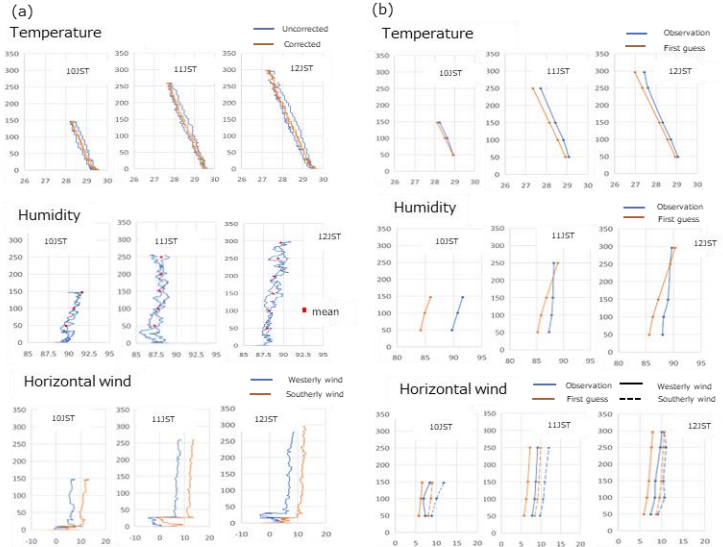


Fig. 5 (a) (upper) Observed vertical profiles of temperature before and after correction. Observed vertical profiles of (middle) humidity and (bottom) horizontal wind. (b) Observed vertical profiles used in the assimilation and first guess vertical profiles of (upper) temperature, (middle) humidity, and (bottom) horizontal wind.

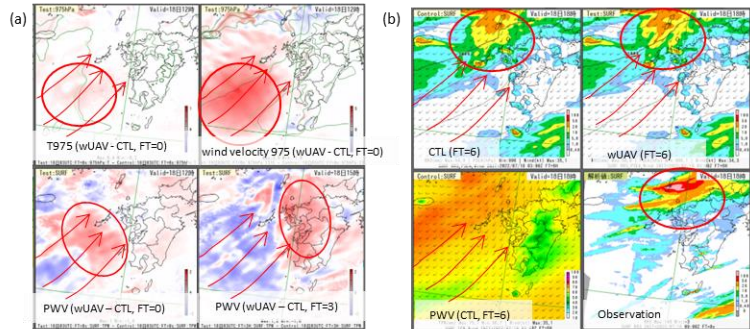


Fig. 6 (a) Differences of (upper left) temperature and (upper right) wind speed of 975 hPa height at FT=0 obtained with small UAV data (wUAV) and without small UAV data (CTL). Differences of PWV between wUAV and CTL at (bottom left) FT=0 and at (bottom right) FT=3hours. (b) 3hour precipitations of (upper left) CTL and (upper right) wUAV. (bottom left) PWV distribution of CTL at FT=6hours, and (bottom right) observed rainfall region at 18JST (the same time of FT=6hours).

# Operational use of hyper spectral infrared sounder radiance data in JMA's meso-scale NWP system

SHIMIZU Hiroyuki

Numerical Prediction Development Center, Japan Meteorological Agency

E-mail: shimizu\_h@met.kishou.go.jp

## 1. Introduction

Operational assimilation of hyper spectral infrared sounder (HSS) radiance data from the Cross-track Infrared Sounder (CrIS) and Infrared Atmospheric Sounding Interferometer (IASI) in JMA's meso-scale Numerical Weather Prediction (NWP) system began on 28 March 2023. This report briefly outlines related channel selection and effects of HSS radiance data assimilation in the meso-scale NWP system.

## 2. Channel selection and quality control

Observation error settings and quality control processes such as cloud detection for HSS radiance data assimilation were implemented in the same manner as those for the global NWP system (Okagaki 2015, Kamekawa and Kazumori 2017). Not all the channels used in the global system are used in the meso-scale system because the meso-scale model top is lower than that of the global system. The height of meso-scale model top is approximately 5 hPa, and the atmospheric profiles above it are extrapolated for radiative transfer calculation using U.S. Standard Atmosphere lapse rates. However, the extrapolated profile is not sufficiently accurate, especially for higher-peaking channels. Differences in calculated brightness temperatures between the global and meso-scale systems were examined to determine the accuracy of radiative transfer calculation in the meso-scale system. Figure 1, which shows histograms of first guess (FG) departures in each system and the weighting functions of corresponding channels, indicates that biases of FG departure were farther from zero for higher-peaking channels, and that standard deviations were larger than those in the global system. For lower-peaking channels, the standard deviations and biases of FG departure are close to those in the global system. Such channels were considered to be less sensitive to layers above the model top of the meso-scale system and were selected for assimilation.

Preliminary experiments were conducted to evaluate the effects of the selected channels. The control experiment (CNTL) had the same configuration as JMA's operational meso-scale NWP system as of March 2022. In the TEST (a) experiment, CrIS assimilated channels were selected subjectively with reference to weighting function (green and red lines in Fig. 2 (c)), and TEST (b) was similar but with assimilated channels (red lines in Fig. 2 (c)) selected based on the FG departure statistics described above. Figures 2 (a) and (b) show that the standard deviation of FG departures against CNTL were larger for clear-sky radiance (CSR) data and microwave sounder data, indicating lower FG accuracy. FGs for TEST (b) were closer to observation values than those of CNTL. These results highlight the importance of removing channels that are even slightly sensitive to atmosphere above the model top.

## 3. Effects of humidity channel assimilation

In addition to usage of the temperature channels described in Section 2, we selected humidity channels via sensitivity analysis based on a Jacobian matrix, and extracted 9 channels considering inter-channel error correlations. These channels were confirmed to be less sensitive to extrapolated profiles above the model top. The effects of their assimilation were evaluated in data assimilation experiments with JMA's meso-scale NWP system. The experimental periods were 26 June 2020 to 31 July 2020 and 18 Dec. 2019 to 31 Jan. 2020. The CNTL experiment had the same configuration as JMA's operational meso-scale NWP system as of March 2022. In TEST (i), CrIS and IASI temperature channels were additionally assimilated to CNTL. In TEST (ii), the selected humidity channels were also assimilated in addition to those of TEST (i).

Figure 3 shows changes in the standard deviation of FG departures against CNTL. FGs in TEST (i) were closer to observation values than those of CNTL for sensors sensitive to humidity and temperature in the troposphere such as microwave imagers and sounders, indicating improved FG accuracy. TEST (ii) exhibited further improvement in FG departure, especially in humidity-sensitive observation such as MHS, GMI and SSMIS. These results indicate that HSS humidity channel assimilation has a positive impact on humidity fields in FGs.

#### 4. Summary

JMA has begun to assimilate HSS radiance data in its meso-scale NWP system. It was found that channel selection in consideration of model top height is important for effective assimilation of HSS radiance. Water vapor channel assimilation also has positive effects on the humidity fields in FGs.

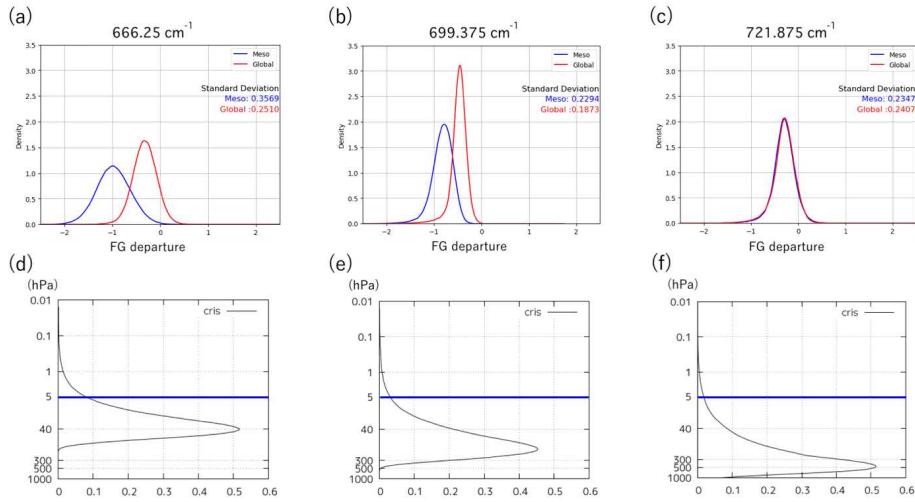


Figure 1: Histograms of CrIS FG departures [K] in the global system (red lines) and the meso-scale system (blue lines). (a) Channel 27 ( $666.25 \text{ cm}^{-1}$ ), (b) channel 80 ( $699.375 \text{ cm}^{-1}$ ) and (c) channel 116 ( $721.875 \text{ cm}^{-1}$ ). (d), (e), (f): weighting functions [unitless] for each channel corresponding to (a), (b) and (c) respectively.

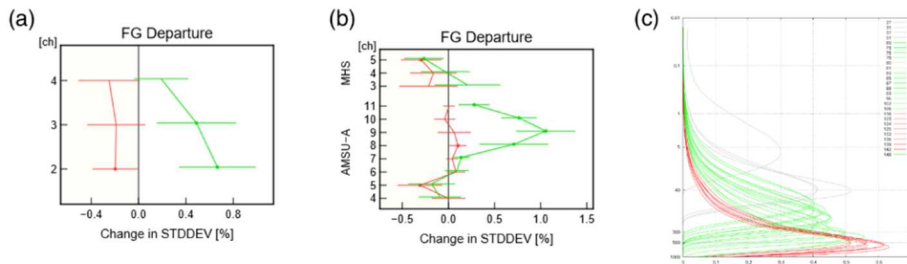


Figure 2: Normalized changes in standard deviation for FG departures in (a) CSR radiances from Himawari-8 and (b) MHS and AMSU-A radiances. Error bars show confidence levels of 95%. Green lines: TEST (a); red lines: TEST (b). (c) Weighting functions of assimilated channels in TEST (a) and TEST (b).

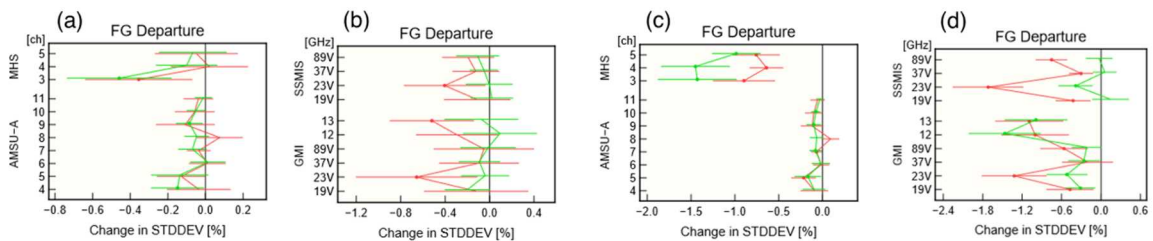


Figure 3: Normalized changes in standard deviation for FG departures of (a) MHS and AMSU-A radiances and (b) GMI and SSMIS radiances in TEST (i). (c) and (d) are as per (a) and (b), but for TEST (ii). The monthly validation periods are July (red dots) and January (green dots) 2020.

#### References

- Okagaki, A. (2015). Assimilation of IASI and AIRS radiances at JMA. *CAS/JSC WGNE. Res. Activ. in Atmos. Oceanic Modell.*, **45**, 1.17-1.18.
- Kamekawa, N. and M. Kazumori. (2017). Assimilation of Suomi NPP/CrIS radiance data into JMA's global NWP system. *CAS/JSC WGNE. Res. Activ. in Atmos. Oceanic Modell.*, **47**, 1.17-1.18.

# Operational Use of Surface Humidity Observations in JMA's Mesoscale NWP Systems

TOGUCHI Ryo, IRIGUCHI Takeshi

Numerical Prediction Development Center, Japan Meteorological Agency

E-mail: r-toguchi@met.kishou.go.jp

## 1. Introduction

Water vapor in the lower troposphere has a significant influence on the occurrence and development of torrential rainfall caused by stationary linear mesoscale convective systems. Accordingly, assimilation of observation data that capture the inflow of lower-tropospheric water vapor is critical for the enhancement of torrential-rain forecasting. In this context, the Japan Meteorological Agency (JMA) observes screen-level relative humidity nationwide at SYNOP weather observation sites, and assimilates the results into its Local NWP System (JMA, 2023). To help clarify the characteristics of such vapor, the Agency incorporates hygrometers in its Automated Meteorological Data Acquisition System (AMeDAS) on a national basis, and has observed relative humidity since 2021. Assimilation of these observation data is expected to enhance the representation of lower-tropospheric water vapor and precipitation forecast accuracy.

JMA began operational assimilation of surface humidity data from the AMeDAS and SYNOP observation stations in its Mesoscale NWP system in March 2023. This paper describes data quality and related effects on precipitation forecasts.

## 2. Quality control (QC) for surface humidity data

The QC algorithm for AMeDAS surface humidity data is based on the existing process for SYNOP surface humidity data in JMA's local NWP system, where conventional humidity data are used. In addition, we introduced the dynamic QC and space consistency checking (Onogi 1998) for humidity observation in this algorithm. Observation errors and other factors for QC are recalculated from the results of observation minus background (O-B).

As AMeDAS does not collect the surface pressure data necessary for conversion of observed relative humidity to specific humidity (a variable in the assimilation system), surface pressure from the first guess (background) is used as an alternative.

## 3. Quality of new surface humidity data

Statistical comparison was conducted between AMeDAS humidity data and the already-established SYNOP data, including mean and standard deviations of O-B, for the period from August to December 2022. The results showed that AMeDAS data exhibit a wet bias to SYNOP data in summer, but the difference was smaller than standard O-B deviation. The statistics also showed sufficient quality for AMeDAS humidity data assimilation. However, the O-B statistics suggested that dry bias in the first guess to surface humidity observation is still present in summer, while surface humidity prediction accuracy with the Meso-Scale Model (MSM) was significantly improved for March 2022 (Sawada et al. 2022).

## 4. Effects on analysis and prediction

To evaluate the effects of the new humidity observation data on the Mesoscale NWP system, numerical experiments have been conducted based on the system since March 2022 (CNTL) with surface humidity observation data (TEST) for July 2021 and January 2022. Data assimilation resulted in a statistically significant improvement in surface humidity forecasts for both summer and winter (Fig. 1). For precipitation prediction, improvement was particularly pronounced where surface humidity observation data were assimilated upstream of heavy-rainfall areas. For 15 UTC on July 15 2022 as the initial MSM forecast time, accuracy for heavy precipitation improved in the 12-hour forecast because the assimilation of surface humidity data increased upstream precipitable water vapor (PWV) values, and vapor from these areas flowed to rainy areas (Fig. 2).

## 5. Summary

In relation to JMA's introduction of new hygrometers for AMeDAS sites all over Japan, this study clarified that the produced surface humidity data was of sufficient quality for assimilation. The introduction of these data for AMeDAS and SYNOP stations also improved forecast accuracy for surface humidity and precipitation in the Mesoscale NWP system. JMA began assimilation of these data in March 2023.

## References

Japan Meteorological Agency, 2023: Data Assimilation Systems, OUTLINE OF THE OPERATIONAL NUMERICAL WEATHER PREDICTION AT THE JAPAN METEOROLOGICAL AGENCY, 9-51.

Onogi, K., 1998: A Data Quality Control Method Using Forecasted Horizontal Gradient and Tendency in a NWP System: Dynamic QC., Journal of the Meteorological Society of Japan, Vol. 76, No. 4, pp. 497-516, 1998.

Sawada M., KITAMURA Y., MATSUBAYASHI K., KUSABIRAKI H., NISHIMOTO S., AIKAWA T., YAMASAKI Y., 2022: Extending Forecast Range and Introducing an Ocean Mixed Layer Model in JMA's Mesoscale NWP System., WGNE Research Activities in Earth System Modelling 2022.

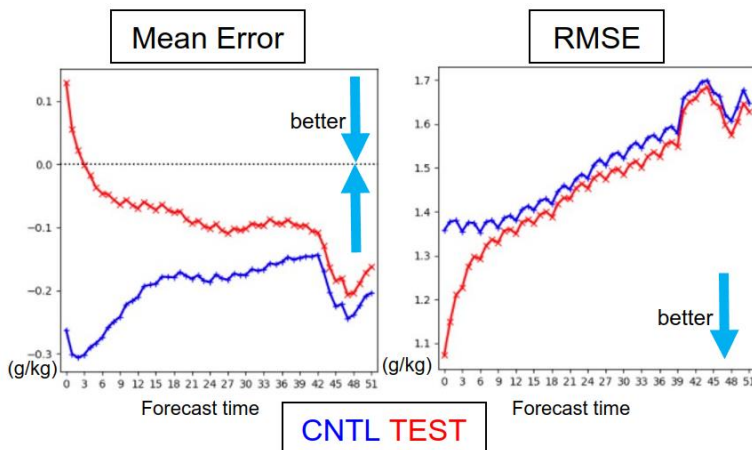


Figure 1. Mean errors and RMSEs for observation of specific humidity [g/kg] over the experimental period of July 1 – 31 2021. Blue lines: CNTL; red lines: TEST.

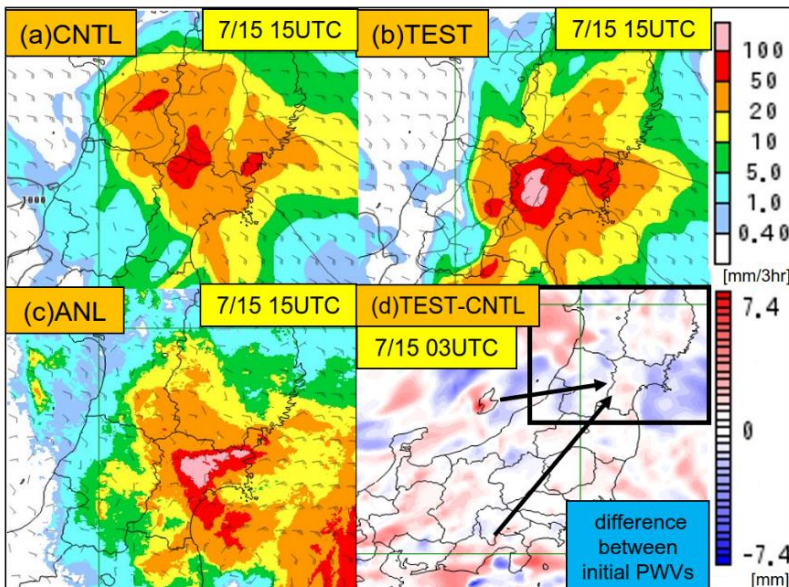


Figure 2. 3-hour cumulative precipitation [mm/3 hrs] at 15 UTC on July 15 2022. (a) TEST (9-hour forecast range), (b) CNTL (9-hour forecast range), (c) radar raingauge analysis precipitation, (d) difference between initial conditions of PWV [mm] (TEST – CNTL) at 03 UTC on July 15 2022. Arrows represent high-humidity air flow.

# The Impact of Dropsonde Data on GFS Forecasts from 2022-2023 Atmospheric River Reconnaissance

Xingren Wu<sup>1</sup>, Keqin Wu<sup>2</sup>, Vijay Tallapragada<sup>3</sup>, and F.M. Ralph<sup>4</sup>

<sup>1</sup>Axiom at EMC/NCEP/NOAA, College Park, MD 20740, <sup>2</sup>Lynker at EMC/NCEP/NOAA, College Park, MD 20740, <sup>3</sup>EMC/NCEP/NOAA, College Park, MD 20740, <sup>4</sup>CW3E, Scripps Institution of Oceanography, UC San Diego, CA 92093

Email: Xingren.Wu@noaa.gov

## 1. Introduction

Atmospheric Rivers (ARs) are a global weather phenomenon that are responsible for most of the water vapor fluxes outside of the tropics and a major source of precipitation and water supply for the U.S. West Coast. AR Reconnaissance (ARR) directly supports critical water management and flood control objectives in the western United States (Ralph et al. 2020). ARR observations are now officially part of the U.S. National Winter Season Operations Plan (NWSOP). During the winter of 2022-2023 AR Recon campaigns, there were 39 successful Intense Observing Periods (IOPs) using Air Force WC-130 flights and NOAA G-IV flights, which provided additional data by supplementing conventional data with dropsonde observations of the full atmospheric profile of water vapor, temperature, and winds within and around ARs. Near real-time data impact experiments had been carried out with the National Centers for Environmental Prediction (NCEP) operational global forecast system (GFS) version 16 (GFSv16) during the 2022-2023 ARR to examine and document the dropsonde impact, including landfalling ARs and associated precipitation.

## 2. Model and Experiments

In this study the NCEP operational GFSv16 was used to examine the impact of the ARR supplemental dropsonde observations on GFS forecasts during the winter of 2022-2023 ARR, including 39 successful IOPs from 5 November 2022 to 14 March 2023.

GFSv16 is the NCEP operation system, with the finite volume cubed-sphere dynamical core and improved GFDL microphysics. The model has 127 vertical layers, with the model top at 80 km, and a horizontal grid with 13 km resolution. The data assimilation (DA) system uses a 4-Dimensional Incremental Analysis Update (4D-IAU) technique. The dropsonde data collected from the 39 IOPs during the ARR 2022-2023 campaign are assimilated in the operational (OPR) run. Global denial (DENY) experiments were conducted by denying the dropsonde data in the GFSv16 for both DA and model forecast.

## 3. Results

The standard NCEP *Metplus* verification system is used to evaluate the DENY experiment against the OPR run. Overall the global verification metrics are very similar between the two runs, with slightly better overall forecast skill (1-5 days) noted over the Pacific North American (PNA, 180-320E, 20-75N) region when the supplemental dropsonde data were used in OPR. The most significant improvement is for the temperature (99% significance) and wind (99.9% significance) forecast at 200hPa with a 72-hour lead, when the mean absolute error (MAE) reduced by about 2.5% each (not shown).

One objective of this study is to examine and document the impact of the dropsonde on the GFS forecast skill of landfalling ARs and the associated precipitation. The MAE of GFS precipitation forecast over the U.S. West Coast

domain (as in Lord et al. 2023) is calculated from the 39 IOPs. The difference of precipitation MAE (DENY-OPR) from 48-72-h forecast is shown in Fig. 1. There are more improvements (positive values) than degradation (negative values) from the 39 IOP cases. The average reduction of MAE for all IOPs is 3.5%. Most of the improved forecast cases are associated with improvement of the moisture forecast and AR landfalling in OPR (not shown).

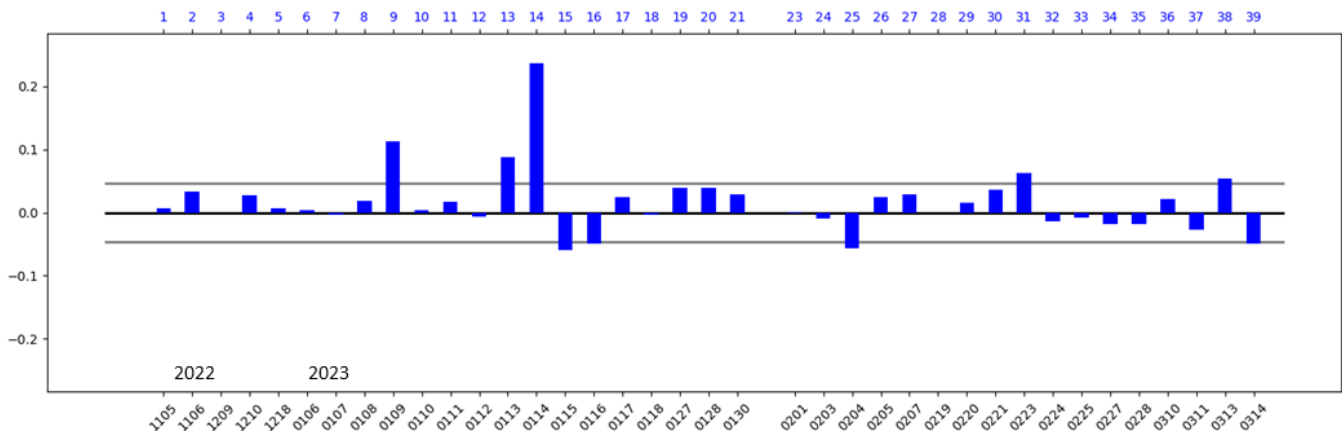


**Figure 1.** The accumulated 24-h precipitation MAE difference (DENY-OPR, inches) from 48-72-h GFSv16 forecast in each of the 39 IOPs from 5 November 2022 to 14 March 2023 averaged over U.S. West Coast domain (107-127 W, 28-49.5 N). The Stage IV precipitation is used as the truth, where the accumulated 24-h precipitation is at least 0.5 inches are used for the forecast verification (IOP 22 is void, i.e. the precipitation from Stage IV is less than 0.5 inches). The gray line is the 95% significant level based on all the IOP cases.

#### 4. Summary

This study indicates that there is a positive dropsonde impact on the GFS forecast skill (1-5 days lead) during the 2022-2023 ARR. The ARR observations helped fill the data gaps needed for DA to provide better model initial conditions (Zheng et al. 2021), with reduced cold bias for the temperature, dry bias for the specific humidity, and low bias for the wind. The improved initial conditions set up a more accurate environment for predicting the AR and associated precipitation. The systematic improvement for the precipitation prediction over the U.S. West Coast, in particular with 48-72-h lead, is associated with improvement in the moisture and water vapor transport forecast, which also leads to improvement in AR landfalling, for the location and IVT (integrated water vapor transport) magnitude, with reduced error in the OPR run. The improved precipitation forecast over the U.S. West from the 2022-2023 ARR is similar to that of ARR 2020 study with GFS version 15 (Lord et al. 2023).

#### Reference:

- Lord, S.J., X. Wu, V. Tallapragada, and F.M. Ralph, 2023. The Impact of Dropsonde Data on the Performance of the NCEP Global Forecast System during the 2020 Atmospheric Rivers Observing Campaign. Part I: Precipitation. *Weather and Forecasting*, **38**, 17–45.
- Ralph F.M., and Coauthors, 2020: West Coast forecast challenges and development of Atmospheric River Reconnaissance. *Bulletin of the American Meteorological Society*, **101**, E1357–E1377, <https://doi.org/10.1175/BAMS-D-19-0183.1>.
- Zheng M., L.D. Monache, X. Wu, F.M. Ralph, B. Cornuelle, V. Tallapragada, J.S. Haase, A.M. Wilson, M. Mazloff, A.C. Subramanian, F. Cannon, 2021: Data Gaps within Atmospheric Rivers over the Northern Pacific. *Bulletin of the American Meteorological Society*, **102**, E492–E524, <https://doi.org/10.1175/BAMS-D-19-0287.1>. 2021.